POLITECNICO DI MILANO

Scuola Di Ingegneria Industriale e dell'Informazione
Dep. of Aerospace Science and Technology
M. Sc. Degree in Aeronautical Engineering

POLITECNICO
MILANO 1863

Impact of Combinations of Wind Farm Controllers on Wind Turbine Loads

Supervisor
Prof. Alessandro CROCE
Co-Supervisor
Prof. Stefano CACCIOLA

Author
Gianluca Dadda - 926956

Academic Year 2020-2021

Abstract

Research of strategies to reduce cost of energy for wind generators resulted in the construction of wind farm increasingly bigger. But although the lower distance reduces installation and maintenance costs, some turbines might operate inside the wake produced by another generator, resulting in lower energy production, as well as higher deterioration of the components. A promising solution to this problem is to introduce a wind farm controller which coordinates the single machines to increase the overall energy harvested. However, while some of these strategies show an increase in energy efficiency, the negative effect they have on the structure might break safety boundaries, requiring a redesign of the turbine in order to withstand the increase in loads given by the controller. This Thesis investigates the possible combination of two different wind farm controllers: one based on deflecting the wake away from downstream turbines by imposing a yaw angle, with an increase on overall energy production at the cost of the upstream turbine, which experiences an increase in loads. The second aims at down-regulating the front row machine to reduce wake effects, and at the same time, the loads on the controlled turbine. The goal is to determine whether a combination of the two is able to keep the load envelope unchanged with respect to the uncontrolled turbine, such that is possible to safely install the wind farm controller on already existing plants. The research has been performed by adopting the aeroservoelastic solver Cp-Lambda, which represent the state of the art in wind turbine design, on a 10MW machine, following procedures akin to modern certification requirements. The focus went on the upwind turbine which is being controlled and how different configurations of the two strategies affect the key performance indicators. Results show that such combination can be advantageous, in fact even a small reduction in power below 6% is sufficient to balance the negative effect on the blade loads brought by the yaw-based control. However, the same cannot be said for tower and hub loads, where down regulating is not enough to counter the effects of the misalignment.

Sommario

La ricerca di strategie per ridurre il costo dell'energia dei generatori eolici ha portato alla costruzione di parchi eolici sempre più grandi e compatti. Mentre la vicinanza riduce i costi, alcune turbine si possono trovare nella condizione di operare all'interno della scia generata da un generatore vicino, con una minore produzione energetica e un maggior deterioramento della macchina. Una soluzione è quella di introdurre un controllore del parco eolico che coordina le turbine in modo da aumentare la produzione complessiva. Tuttavia, mentre alcune strategie mostrano un incremento in efficienza elettrica, l'effetto che hanno sulla struttura della macchina porta a implicazioni sulla sicurezza, richiedendo un redesign della turbina eolica in modo da sostenere l'incremento nei carichi portato dal controllo. In questa Tesi si è investigata la combinazione di due diversi controlli di wind farm: il primo basato sul deviare la scia lontano dalle altre turbine imponendo un angolo di imbardata, aumentando l'efficienza del parco eolico a scapito della turbina a monte, la quale vede un aumento dei carichi. Il secondo si basa sul depotenziare la macchina in prima fila in modo da ridurre gli effetti di scia, e allo stesso tempo, i carichi. L'obbiettivo è quello di stabilire se, combinandole, fosse possibile mantenere i carichi invariati rispetto alla turbina senza controllo, in modo da poter installare le logiche in parchi eolici già esistenti. La ricerca è stata effettuata utilizzando il risolutore aeroservoelastico Cp-Lambda su una macchina da 10MW in modo affine alle procedure di certificazione vigenti. L'attenzione è stata posta sulla turbina a monte su cui verrebbe attivato il controllo e su come diverse combinazioni delle due strategie impattano sugli indicatori di prestazione chiave. I risultati dimostrano che la combinazione può essere vantaggiosa, infatti anche un depotenziamento inferiore al 6% è sufficiente per bilanciare l'effetto sui carichi della pala introdotto dal controllo di imbardata. Tuttavia, lo stesso non si può dire per la torre e l'hub, dove l'introduzione del depotenziamento non è sufficiente per contrastare gli effetti del disallineamento.

Acknowledgements

Prima di presentare il lavoro compiuto durante questa tesi di laurea magistrale, vorrei porre i miei ringraziamenti a coloro che hanno contribuito e mi hanno sostenuto lungo questo percorso.
Innanzitutto, ringrazio il professor Alessandro Croce per aver reso possibile questo progetto, fornendomi gli strumenti e le conoscenze utili al suo svolgimento. Inoltre vorrei ringraziare Stefano Cacciola, che si è sempre reso disponibile durante il lavoro.
Ringrazio i miei genitori, Cinzia e Giancarlo, per il supporto che hanno dimostrato durante tutto il mio percorso di studi, sopportandomi nei periodi piu difficili e fornendomi il loro aiuto quando possibile.
Vorrei ringraziare Letizia, che c'è sempre stata, e mi ha fornito sempre il suo supporto lungo questo percorso di studi.
Infine, ringrazio tutti i miei numerosi amici, che sono sempre stati disponibili e con cui ho passato dei bellissimi momenti, e che sono stati sempre presenti per risollevarmi il morale nei periodi piu difficili.

Contents

List of Figures

List of Tables

Chapter 1

Introduction

Over the last decades, interest towards clean and renewable energy has increased steadily in order to replace fossil fuel and slow down climate change before it deals irreversible damage to he planet. The Paris agreement aims to keep global warming well below 2°C, ideally limited to 1.5°C. To do so, energy production must move away from fossil fuel towards cleaner and renewable sources. Among all of them, wind energy may play a leading role in this transformation, for his high accessibility and competitive cost of energy (CoE) with respect to other green energy sources. In fact, according to IRENA [1], in 2018 onshore wind CoE is on average of 0.06 USD/kWh, while offshore CoE fluctuates around 0.13 USD/kWh due to the higher installation and maintenance costs. Although wind energy is already one of the cheapest renewable sources, this is not stopping research from both the academic and industrial environments to bring the CoE even lower. Instead is quite the opposite, as it is accounted for 63% of Europe's investments in 2018 [2].

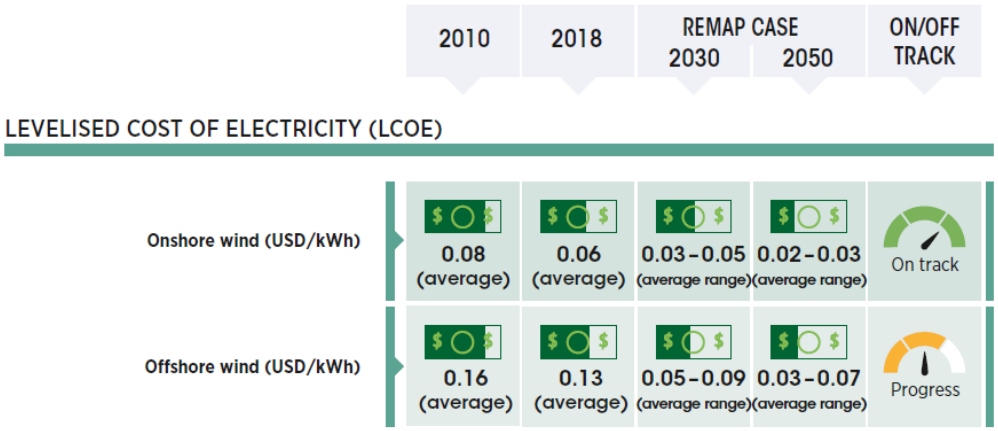

Figure 1.1: *The cost of wind energy, present and future. Credit to IRENA [1].*

One way to increase cost efficiency is to cluster together many wind turbines in the same site, hence the name wind farm, reducing the operational costs. However, given the nature of the wind resource, each wind turbine has an influence on the others, especially when some of them are operating inside the wake of an upwind machine, experiencing a slower yet more turbulent flow, and a consequent increase in fatigue loads and decrease in power production. Traditional wind plants let turbines operate on their own, according to the control system they have installed, which is tuned to optimize the power production by chasing the optimal power coefficient for any given wind condition, without taking into account the presence of nearby wind turbines. As the number of wind farms, both onshore and offshore, is increasing over the years and this trend is expected to continue in the future [1], the concept of wind farm control (WFC) has become an hot topic in the wind energy community. Acting as a supervisor of the plant, the WFC aims at increasing the overall power production by reducing the wake interactions between the turbines. Generally, this is achieved operating some machines, usually the upstream ones, in a non optimal state, but in a way such that other turbines can harvest more energy, resulting in a net increase in production. Nowadays different wind farm control strategies are being developed as a possible way to increase wind farm efficiency. However, while research has shown the potential benefits in power production for some strategies, other results highlight an increase in ultimate loads, tip deflection and fatigue loads on the controlled turbine with dangerous safety implications that might require a redesign of the blade's structure to take into account for the higher loads, which leads to an increase in blade mass and therefore, rotor cost. Another strategy, called axial induction control, operates the front row turbine at lower power, reducing the wake effects. In this case, studies have shown that this strategy lowers the loads of the controlled machine, but with no meaningful gain or loss in wind farm power production. The scope of this thesis is to investigate the combination of yaw based WFC with induction control, focusing on the effect they have on the operated turbine in terms of loading and power production, to understand if such combination could avoid the need of a blade redesign while still maintaining the benefits in power production brought by the WFC.

1.1 Scope and methodology

The number of installed wind farms has seen a large increase in recent years, especially off shore [2], with many more commissioned for future years. The driving advantages are the reduced installation cost while increasing power production per unit area. While this lowers the CoE with respect to a single wind turbine, installing them closer together means that the interaction between single machines

cannot be overlooked anymore. Each turbine produces a wake, i.e. a region of turbulent flow, downwind of the rotor, with lower energy in relation to undisturbed wind. For some wind directions, this wake can invest a downstream turbine, decreasing their energy production while at the same time increasing their degradation due to the higher turbulence [3]. A study from Barthelmie et al. estimate a power loss of about 12% with respect to an individual turbine [4], while for a low-spaced wind farm like Lillground it has been estimated to be around 23% [5]. Because of this, wind farm control techniques are being developed to bring down the overall energy loss. Among all possible solutions under study, one of them is called axial induction control, where wake effects are reduced by down-regulating upstream turbines, effectively operating them at sub-optimal power setting, but with an increase in production for the turbines behind. However, as shown by many studies, the overall benefit in power production is near zero [4]. The real benefit of this strategy, as shown by Santoni et al. [6], is a reduction in turbine loading while maintaining an equivalent power production at the farm level. Another technique is to steer the wake by operating the upwind turbine in a misaligned state, not perpendicular to the flow such that its wake is deflected away from downwind machines, hence the name Wake Redirection (WR). In this regard, research has shown that for certain misalignment the overall production of the plant can increase despite the power loss of the controlled turbines [7]. The downside of WR is that by being at a constant yaw angle with respect to the wind direction, the controlled turbine experiences an increase in loads [8]. In modern wind turbine design, some loads or displacements are treated as active design constraints, which are kept as tight as possible to reduce structural costs, that even a small increase in such values can be out of the operational envelope with serious safety implications, thus requiring a structural redesign of the turbine to safely operate this WFC strategy, with an increase in blade mass which reflects on the CoE. For this reason, the combination of the two control logic might be advantageous, where axial induction control load reduction should theoretically complement for the increase brought by WR, while increasing the plant overall production. The purpose of this study is to investigate how these combined laws work together for different setup combinations and how they modify ultimate and fatigue loads on the controlled turbine with respect to standard control. To do so, we employed the aero-servo-elastic solver Cp-Lambda, developed by the Aerospace Engineering department at Politecnico di Milano, which represents the state of the art for what concerns wind turbine design to get the most realistic and accurate results possible. In this regard, the parametric analyses have been performed on the 10MW reference turbine developed by DTU [9], a well known turbine used for many other studies on wind energy.

1.2 Outline of the Work

This thesis is organized as follows: Chapter 2 provides a brief overview of the modern wind farm control strategies to give context to this work. Chapter 3 describes the baseline wind turbine model and controller used to perform the parametric analysis, providing the benchmark values in terms of ultimate and fatigue loads, and the work-environment tools adopted. Chapter 4 deals with the main topic of this Thesis, here we present the results of the parametric analysis on the different configurations on the two aforementioned WFC strategies and the impact it has on the wind turbine's key performance indicators for each of the combinations under study. In particular, we show the possible benefits and drawbacks brought by these wind farm controls. Lastly, chapter 5 draws conclusions on the main results, as well as potential future developments.

Chapter 2

Wind farm control strategies

In order to keep global warming under the international agreements threshold, renewable energy should grow from the 20% of global energy generation measured in 2018 to 67% by 2050. Given his numerous advantages over other renewable sources, especially economical, wind might lead this conversion to green energy. However, to achieve such a huge conversion, wind farms must increase in number significantly, but since the number of sites with strong and reliable wind resource is limited, eventually new plants will have to be built in regions with less available energy. To balance this, wind farms must find a way to become more efficient at energy production.
In modern wind farms each turbine operates a control system which seeks to maximise its production. This is ideal when considering an isolated machine, but in the framework of a wind farm, mutual interaction between turbines can't be ignored anymore. In fact, for some wind directions, a turbine may operate inside the wake produced by an upwind rotor. The wake is a region of altered flow which arises behind the body invested by the flow and extends for some distance. It is associated with the following phenomena:

- Velocity deficit, resulting from the energy extraction of the turbine.
- Increased turbulence intensity, caused by the blade's rotation and vortex tips.
- Recovery, where the wind velocity recovers the free stream velocity due to mixing.
- Meandering; i.e. a stochastic phenomenon in which the wake centre shows horizontal and vertical oscillations.
- Expansion, i.e. the area of the wake increases with respect to the distance from the turbine.

- Deflection, occurring when the rotor is not perpendicular with respect to the free flow.

- Vertical wind shear, the flow field's properties vary vertically inside the wake.

These effects have an impact on wind turbines both in terms of production losses and an increase in ultimate and fatigue loads. Regarding the first issue, studies have estimated a total loss from 10% to 25% of annual power production due to wake effects [4][5], depending on the relative position and distance of the turbines. Figure 2.1 shows the power deficit with respect to wind direction for the low-spaced Lillground wind farm.

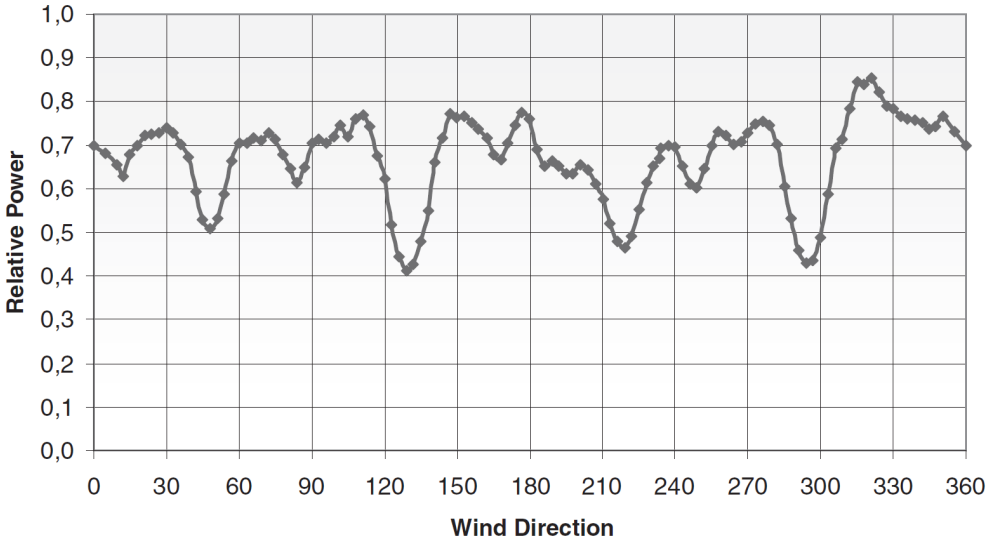

Figure 2.1: *Lillground wind farm: variation in array efficiency with wind direction for wind speeds below rated. Credit to Dahlberg and Thor [10].*

While for the second issue, it has been demonstrated that operating inside a wake yields a significant increase in loads even for long distances form the upwind turbine [3]. For these reasons, the interest towards the development of wind farm control strategies has risen over recent years. The controller acts as a supervisor over the entire plant, accounts for the interactions between each of them and coordinates the operation of the machines to achieve the best performance for the farm. This means that for a given wind direction, some turbines may operate in a non-optimal condition, sacrificing their own performance to improve the performance of others which would operate under maximum wake effects otherwise. Different approaches to wind farm control are possible, in the following sections we provide brief explanations for three of them.

2.1 Axial Induction control

One of the possible solutions for WFC is to simply reduce the axial induction that the upstream turbine has on the wake by down-regulating the machine, thus reducing the thrust and torque forces acting on the blades, as well as the reaction forces acting on the wind, which are generating the wake. There are several ways to implement Axial Induction Control, one of them is to operate the turbine below rated power, also called as derating. The power production of a wind turbine can be described by the following equation:

$$P = \frac{1}{2} A V^3 C_p(\beta, \lambda) \tag{2.1}$$

$$\lambda = \frac{\Omega R}{V} \tag{2.2}$$

Where A is the area of the rotor disk, V the wind speed impinging on the rotor, β the pitch angle of the blades and λ is the tip speed ratio (TSR), an adimensional parameter defined as the ratio between the tip speed and wind speed. Looking at eq. (2.1) it can be clearly seen that once the rotor design is fixed, only the C_p can be modified to change the power.
The power coefficient is dependent on many properties of the rotor and blade design, but also on the pitch angle and tip speed ratio. Modern wind generators are designed to work at the maximum value of C_p for wind speeds below rated, also called as region 2 or partial loading, and at reduced values of this coefficient for wind speeds above rated, region 3 or full loading, such that power remains constant at the design value even for high wind speeds. Thus for each wind speed the optimal value for C_p can be computed and the relative values for the pitch of the blades and rotor speed.
For the purpose of derating, it is possible to find a sub-optimal C_p as an arbitrary percentage of the optimal coefficient, this method is also called as percentage reserve, as it does not extract a portion of the available power from the flow, "reserving" it for downwind turbines. However, while computing the maximum C_p yields a single solution, a lower value can be found for an infinite combination of pitch angle and TSR, for this reason, there are different strategies to implement derating in partial loading, whether one wants to decrease, increase or maintain constant the tip speed ratio that yields the optimal C_p, as can be seen in fig. 2.2. Since the three strategies give similar results regarding the operated machine loading, for this project the third one has been chosen. In region 3 instead, derating can be achieved by simply lowering the rated generator torque or the rotor speed. Again, the impact on the turbine is comparable, so we chose to maintain the original value of the rotor speed.

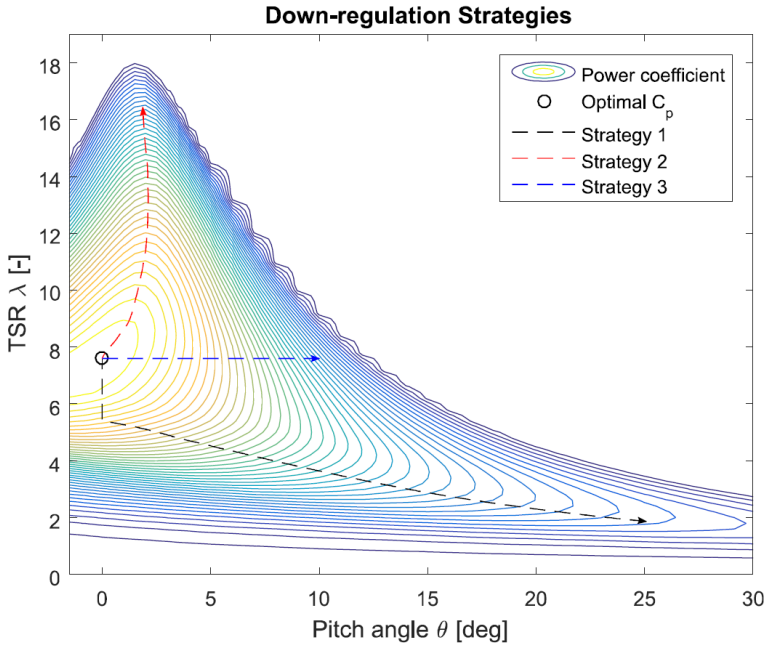

Figure 2.2: *Countour plot of a wind turbine's power coefficient indicating three possible down-regulation strategies in partial load. Credit to CL-Windcon [11].*

Several studies have been performed on axial induction control, especially on the wind farm level, with mixed results. Although initial results showed a potential increase in production [12], more recent studies like the one from Bartl et al.[13] on traditional wind farms, where the distance between upwind and downwind turbines is around seven diameters, show that the power that is not purposely captured by the upstream turbine will not be completely captured by the downstream one. This may be caused by the deviation of the wake between the two machines due to many factors such as:

- wind direction;
- relative position of the turbines;
- wake meandering and expansion;

In fact, for normal operation in turbulent wind, the stream is never perfectly perpendicular to the rotor, leading to a small deviation of the wake, which will not fully invest the turbine behind.
Although this strategy does not bring a meaningful benefit to the overall production of the wind farm, studies focused on it's effects on the single machines show that by down regulating the machine, the loads are lower while maintaining equivalent power production [6].

2.2 Wake steering

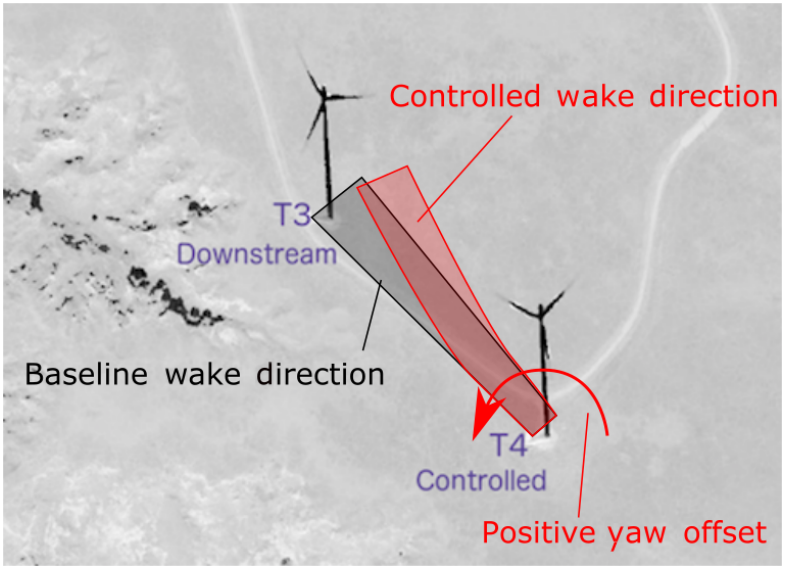

Figure 2.3: *Example of yaw-based steering strategy. Credit to Fleming et al. [14].*

When the rotor is not perpendicular with the wind, lateral and vertical forces are acting on the turbine, and by reaction on the wake, resulting in its deflection, which depends on the misalignment. The wake redirection method exploits this simple phenomena to move the wake away from the downstream machines by orientating the upstream rotor at a given yaw angle with respect to the wind, as presented in fig. 2.3. While the front turbine is working sub-optimally, back row turbine are not working inside a wake, increasing their energy output. In fact, it has been proven that by implementing this control the total energy production of the plant increases, as well as reducing the loads on the downwind machines [15], however the front row turbine is experiencing an increase in loads and, most importantly, a significant increase for the maximum tip deflection [8], which is often an active constraint in the design of modern fiber glass turbines, thus making this WFC strategy not implementable on already existing wind farms where machines are not designed with this control in mind, as it would bring the maximum tip displacement over the maximum allowed.
There are two main ways to implement wake redirection: the first one is to rotate the nacelle yaw or tilt angle by the appropriate value, both showing production benefits from CFD simulation on a 2 turbines configuration performed by Fleming et al [16]. The former is usually preferred since modern wind turbine are already implemented with yaw control to follow changes in the wind directions, making the

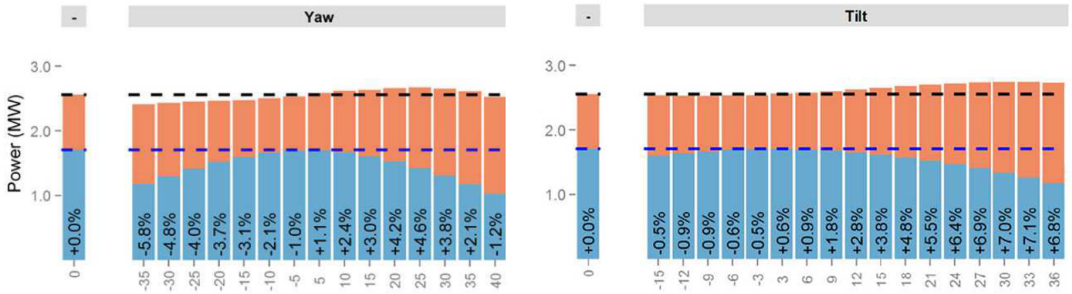

Figure 2.4: *Difference in power output for different configurations. Turbine 1 is blue, turbine 2 is orange. Left plot: yaw misalignment, right plot: tilt misalignment. Credit to Fleming et al. [16].*

implementation of wake steering easier. A comparison of the two is represented in fig. 2.4.
The second way is to use a cyclical pitch input (IPC) to skew the wake horizontally or vertically by introducing a yawing or tilting moment. However this technique is still in early development and not yet optimized, in fact the pitch motion introduces a substantial increase in blade loading while still not achieving the same results of the yaw or tilt misalignment in terms of power increase. In particular, Wang et al [17] have found that yaw steering is able to achieve a more significant lateral wake deflection and consequently, a power increase, with respect to IPC, while the latter provides a faster wake recovery. The difference is visible in fig. 2.5, where the IPC method produces a wake with higher vorticity which promotes the recovery of the wake

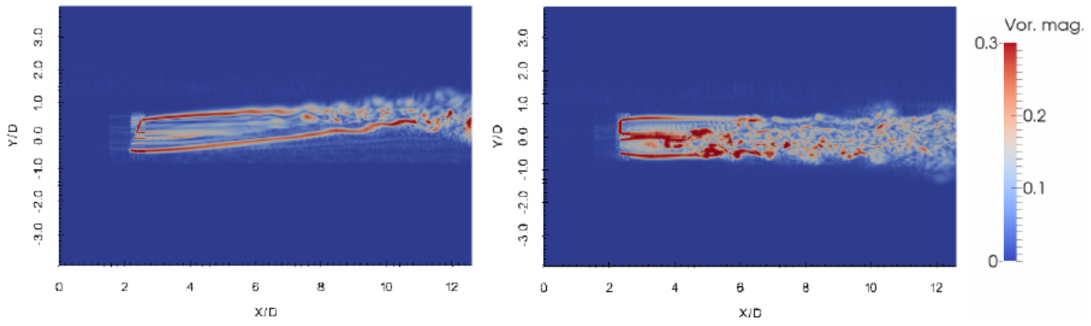

Figure 2.5: *Vorticity magnitude comparison. Left plot: Yaw misalignment, right plot: IPC, image from [17].*

2.3 Dynamic Inducton Control

A novel strategy, proposed by Goit & Meyers [18], based on a cyclic variation of the rotor thrust which has the effect to promote a faster wake recovery through a complex fluid dynamic mechanism. It has been proven that the wake produced by a turbine operating with Dynamic induction control (DIC) has an higher mean velocity, which corresponds to an higher energy yield for an eventual downstream machine.
Dynamic Induction Control can be implemented in a number of ways, one of them is to collectively move the blade's pitch angle periodically, this technique is known as Periodic Collective Motion (PCM). PCM moves the blades following a periodic function given by the user, summing his value to the commanded pitch given by turbine's own control system. Any zero-mean periodic function can work (fundamental to maintain average blade operation around the optimal angle of attack), currently sinusoidal and Gaussian shapes are under study, represented in fig. 2.6, with the latter showing better overall performance.

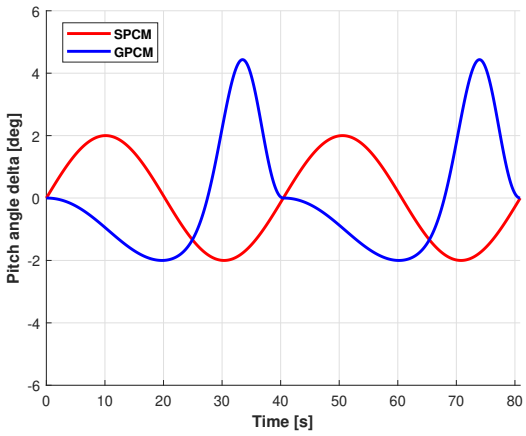

Figure 2.6: *An example of SPCM and GPCM periodic functions.*

The periodic motion of the blades generates an oscillation on the vorticity. This gradient in vorticity brings additional mixing around the zone in which is maximum, breaking the boundary between the wake and the outer flow earlier with respect to the non DIC case, allowing for a faster wake recovery. The higher the gradient, the faster the recovery, and it depends on the difference between the positive and negative peaks in the periodic motion, but while the positive peak can be safely increased, this is not true for the negative peak as it corresponds to a lower pitch angle that can be detrimental in effectiveness and blade loading, as pitch control is mainly used to brake the rotor. This is the main reason of the

Gaussian PCM (GPCM), which adds degrees of freedom on the periodic shape with respect to the sinusoidal PCM (SPCM), allowing for an higher positive peak while maintaining the negative peak relatively small. Regarding the oscillation frequency, it has been found throughout sensitivity studies that the optimal DIC frequency is related with the Strouhal number [19], defined as the frequency at which the vortex rings are shed from the rotor made dimensionless through the ratio between the rotor diameter and undisturbed wind speed. Given the importance of the tip vortices in the wake recovery process, another technique that applies the periodic motion only to the blade tip, called Tip PCM (TPCM) has been tested in a recent study [20], however the results show that TPCM does not provide significant benefits. Figure 2.7 represents the effect of the aforementioned strategies on the mean velocity for different distances from the rotor. Both SPCM and GPCM cases have an higher wake velocity with respect to the baseline configuration, with GPCM showing a better overall performance especially for low distance. It is also noticeable the ineffectiveness of TPCM.

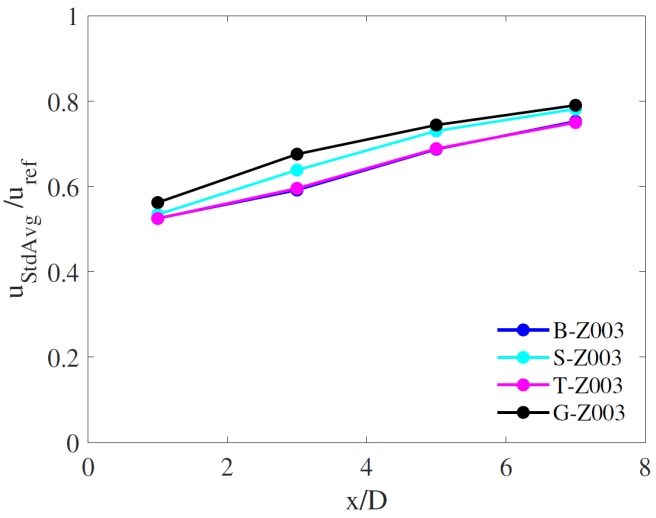

Figure 2.7: *Non-dimensional standard average velocity evaluated at different distances. Baseline: "B-Z003", SPCM: "S-Z003",TPCM: "T-Z003" GPCM: "G-Z003". Image taken from [20].*

Even if this techniques share many similarities with axial induction control, both aiming at reducing wake effects for downstream turbines, DIC does not require the down-regulation of the machine, which will operate in the neighborhood of the optimal condition, hence a smaller impact on the production. In this regard, the potential benefits in production have been studied to be around 5% overall increase for a simple wind farm configuration [19]. On the other hand, DIC has a negative impact on the turbine structure, especially on the fatigue loads due to the oscillatory nature of the PCM [8].

2.4 Combination of different WFC strategies

As explained above, both Wake redirection and PCM control have the downside of an increase in loading and fatigue for the entire system, with the risk of not complying with the maximum allowed for modern wind turbine certification requirements, as most of the time they represent an active design constraint. With this in mind, one can combine the two strategies with Derating, for which has been demonstrated that it reduces blade loading, to cope with the downsides of both WR and PCM, while, hopefully, keeping the benefit of an overall power increase. The scope of this Thesis is to look into the Derating and Yaw control combination, studying different configuration of the two strategies such that it maintains the same or lower loads with respect to the uncontrolled turbine.

Chapter 3

Models and Tools

This chapter describes in detail the reference turbine, it's controller and the tools used to carry out the aerolastic simulations, as well the key performance indicators of the baseline configuration without any wind farm control installed that will serve as benchmark values to evaluate the impact of the WFC strategies.

3.1 Turbine

The turbine used for this project is the DTU 10MW Reference Wind Turbine [9], a model used for a wide range of studies thanks to his peculiar design characteristics and accessibility. It's a traditional three bladed wind turbine designed for offshore sites with IEC wind class 1A with a rated power of 10MW, inspired by the NREL 5 MW reference turbine [21]. The turbine has been designed to provide a reference model used for comparison of both aero-elastic as well as high fidelity aerodynamic and structural tools, equipped with a rotor of good aerodynamic performance and fairly low weight. It's not meant to be manufactured, and while it's design does not push boundaries in terms of weight and safety factors, it serves as a representative design basis for next generation rotors and a description of its components are publicly available. An overall description is provided in table 3.1.

3.1.1 Blade

To design a relatively light-weight rotor, one common way is to increase the relative thickness of the airfoils to stiffen the blade. Thus, the rotor uses FFA-W3-xxx series airfoils, frequently used in modern wind turbine design, for their focus on high relative thickness while still being fairly aerodynamically efficient. Also, their properties are publicly available. In fact, wind tunnel test data exist for the FFA-W3 series, however, those measurement have been carried out at a Reynolds number

Specifics	Values
Class and category	IEC Class 1A
Rated Power	10 MW
Rotor orientation, configuration	Upwind, 3 blades, clockwise rotation
Control	Variable speed, collective pitch
Rotor, hub diameter	178.3 m
Hub diameter	5.6 m
Hub height	119 m
Cut-in wind speed	4 m/s
Cut-out wind speed	25 m/s
Rated wind speed	11.5 m/s
Minimum rotor speed	6 rpm
Rated rotor speed	9.6 rpm
Drivetrain	Medium speed, multiple stages gearbox
Gearbox ratio	50
Rated tip speed	90 m/s
Rotor mass	228 tons
Rotor overhang	7.1 m
Nacelle uptilt, rotor precone	5°
Rotor precone	4.65°

Table 3.1: *DTU 10 MW reference turbine main parameters.*

of Re=1.6x10^6 with high turbulence intensity. Since the influence of the Reynolds number is significant, 2D computations using XFOIL [22] have been conducted between 9x10^6 and 1.3x10^7 and then corrected for 3D effects [23].
They normally range from 24.1% to 36% relative thickness, starting from the tip, then profiles of 48% and 60% relative thickness have been created to interface the FFA-W3-360 and the cylinder at the base, by interpolating the two profiles to ensure smooth transitions. However, due to numerical instabilities in several simulations, the 60% thickness airfoils has been excluded from our reference model and the aerodynamic properties of the blade from the root to the first 48% airfoil have been obtained by direct interpolation. The blade is also twisted with a decreasing angle from root to tip. The main geometrical and aerodynamic parameters of the airfoils are reported in table 3.2 and fig. 3.1.

#	Airfoil	Thickness [%]	Twist [deg]	Spanwise position [%]
1	Cylinder	100	14.50°	0
2	Cylinder	100	14.50°	1.74
3	FFA-W3-480	48	10.08°	20.80
4	FFA-WE-360	36	7.3°	29.24
5	FFA-WE-301	30.1	5.75°	38.76
6	FFA-W3-241	24.1	0.1°	71.78
7	FFA-W3-241	24.1	-3.43°	100

Table 3.2: *List of airfoils on the DTU turbine.*

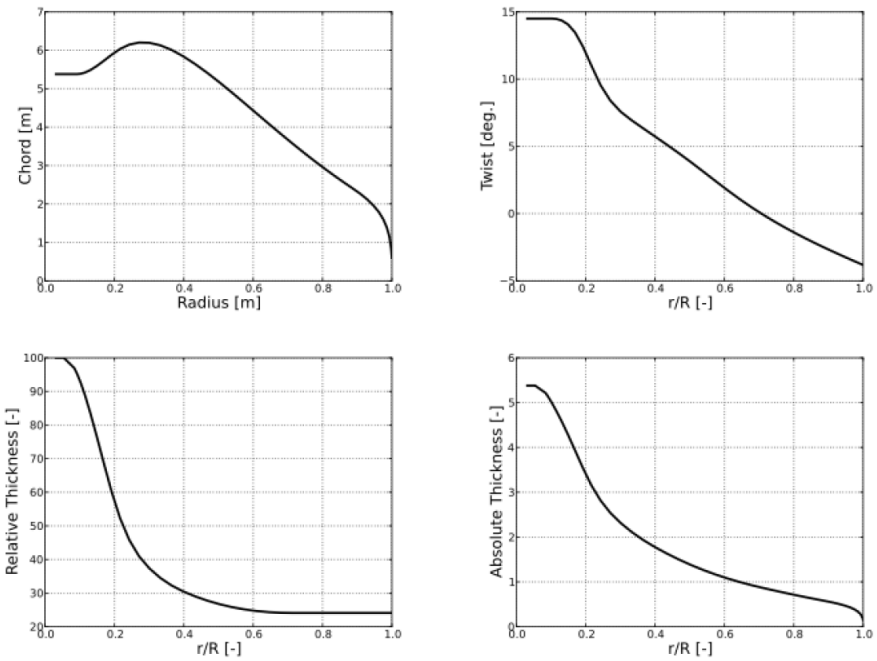

Figure 3.1: *Blade planform aerodynamic parameters. Credit to DTU [9].*

3.1.2 Tower

The tower is 118m tall, made of steel S355. Its external diameter ranges from 8.3m at the bottom to 5.5m at the top. To calculate its structural properties, the mass density has been increased to take into account for the mass of the secondary structures placed inside.

3.1.3 Controller

The turbine is equipped with the PoliWind LQR controlled, which uses the Linear Quadratic Regulator method to derive a control law. It's main advantages over traditional PID or PI control, such as the DTU controller [24] and IK4 OpenWitcon [25], is that it's derived from a reduced and simplified model of the wind turbine capable of capturing the dynamics of the system, also it allows Multi-Input Multi-Output control and it does not need a different treatment for each operating region of the machine, allowing a simple implementation even for turbines with a tip speed constraint [26]. The non linear model adopted is made of the following set of equation:

$$(J_R + J_G)\dot{\Omega} + T_l(\Omega)T_{el_e} - T_a(\Omega, \beta_{el}, V_w - \dot{d}, V_m) = 0 \tag{3.1a}$$

$$M_T\ddot{d} + C_T\dot{d} + K_T d - F_a(\Omega, \beta_e, V_w - \dot{d}, V_m) = 0 \tag{3.1b}$$

$$\ddot{\beta}_e + 2\xi\omega\dot{\beta}_e + \omega^2(\beta_e - \beta_c) = 0 \tag{3.1c}$$

$$\dot{T_{el_e}} + \frac{1}{\tau}(T_{el_e} - T_{el_c}) = 0 \tag{3.1d}$$

Where eq. (3.1a) refers to the drive-train dynamics, eq. (3.1b) describes the tower fore-aft. motion, eq. (3.1c) represents the blade pitch and eq. (3.1d) the torque actuator. For this set of equations, the states are the tower top displacement d and it's derivative $\dot{d}$, the rotor speed Ω, the pitch angle β, pitch rate $\dot{\beta}$ and the electrical torque T_{el}. The control inputs are the commanded blade pitch β_c and electrical torque T_{el_c}.
The rotor thrust and torque coefficients, F_a and T_a, are given by Eqs. 3.2:

$$T_a = \frac{1}{2}\rho\pi R^3 \frac{C_{P_e}(\lambda, \beta_e, V_m)}{\lambda}(V_w - \dot{d})^2 \tag{3.2a}$$

$$F_a = \frac{1}{2}\rho\pi R^2 C_{F_e}(\lambda, \beta_e, V_m)(V_w - \dot{d})^2 \tag{3.2b}$$

$$V_w = V_m + V_t \tag{3.2c}$$

The aerodynamic coefficients C_p and C_f are computed offline by feeding the aerolastic model of the turbine to an aerolastic solver and are stored in look-up tables. Thus, eq. (3.1) can be written in compact form as:

$$\dot{\mathbf{x}} = \mathbf{f}(\mathbf{x}, \mathbf{u}, V_m) \tag{3.3a}$$

$$\mathbf{x}(0) = \mathbf{x}_0 \tag{3.3b}$$

by defining the state and input vectors:

$$\mathbf{x} = (d, \dot{d}, \Omega, \beta_e, \dot{\beta}_e, T_{el_e})^T \tag{3.4a}$$

$$\mathbf{u} = (\beta_c, T_{el_c})^T \tag{3.4b}$$

To proceed in the derivation, given the presence of high order dynamics, a numerical linarization of eq. (3.1) around steady trimmed conditions is needed. To do so, the wind speed has been separated in its mean and turbulent component, allowing to linearize the system around N values of V_m between cut-in and cut-out speeds. The N equilibrium and trimmed conditions are computed by beforehand via the C_p vs TSR vs blade pitch curves and the turbine's data. With this operation it is possible to find the goal regulation states $\mathbf{x}^*(V)$ (or outputs $\mathbf{y}^*(V)$) and control inputs $\mathbf{u}^*(V)$ given in terms of the mean wind speed V_m that can be computed with a moving average of V_w, provided by an on-board anemometer or a hub wind observer.

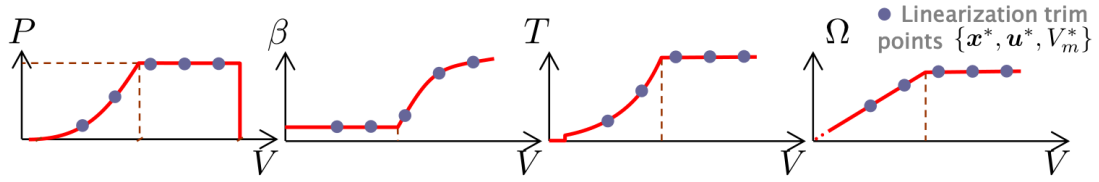

Figure 3.2: *An example of the N trim points parameters.*

Given the N trim points, the reduced model is perturbed around each point, considering $V_t = 0$. Then the linearization can be done through different approaches, such as analytical or numerical methods (i.e. Finite Differences) and the reduced models becomes:

$$\Delta\dot{\mathbf{x}} = \mathbf{A}(\mathbf{x}^*, \mathbf{u}^*, V_m^*)\Delta\mathbf{x} + \mathbf{B}(\mathbf{x}^*, \mathbf{u}^*, V_m^*)\Delta\mathbf{u} \tag{3.5a}$$

$$\Delta\mathbf{x} = \mathbf{x} - \mathbf{x}^* \tag{3.5b}$$

$$\Delta\mathbf{u} = \mathbf{u} - \mathbf{u}^* \tag{3.5c}$$

With the above equation we can write the quadratic cost index J given by:

$$J = \frac{1}{2}\int_0^\infty (\Delta\mathbf{x}^T\mathbf{Q}\Delta\mathbf{x} + \Delta\mathbf{u}^T\mathbf{R}\Delta\mathbf{u})\, dt \tag{3.6}$$

Where $Q >= 0$ and $R > 0$ are symmetric weight matrices that can be tuned to increase the importance of some of the parameters with respect to the others, also,

since the operation is repeated for N wind speeds, they can be wind scheduled. Assuming that all states can be measured or observed, the goal is to find the LQR feedback gain matrix $\mathbf{K}(Vw)$ which requires the minimization of function J. However eq. (3.6) must be constrained to meet the dynamics of the reduced model, by applying the method of the Lagrange multipliers it is possible to unconstrain the optimization problem, which becomes:

$$J = \frac{1}{2}\int_0^\infty (\Delta\mathbf{x}^T\mathbf{Q}\Delta\mathbf{x} + \Delta\mathbf{u}^T\mathbf{R}\Delta\mathbf{u} + \lambda^T(\Delta\dot{\mathbf{x}} - \mathbf{A}\Delta\mathbf{x} - \mathbf{B}\Delta\mathbf{u}))\ dt \tag{3.7}$$

For full state feedback control the solution is in closed form and can be found by solving the Riccati equation of eq. (3.8), which becomes algebraic by assuming a steady state solution for $t \to \infty$.

$$\mathbf{PA} + \mathbf{A}^T\mathbf{P} - \mathbf{P}\bar{\mathbf{R}}\mathbf{P} + \mathbf{Q} = 0 \tag{3.8a}$$

$$\lambda(t) = \mathbf{P}\Delta\mathbf{x}(t) \tag{3.8b}$$

$$\bar{\mathbf{R}} = \mathbf{B}\mathbf{R}^{-1}\mathbf{B}^T \tag{3.8c}$$

Since matrices $\mathbf{A}$ and $\mathbf{B}$ are given by the reduced linearized model computed in a previous step, and matrices $\mathbf{Q}$ and $\mathbf{R}$ are decided by the user, it is possible to solve the above equation and find matrix $\mathbf{P}$. Thus, the gain matrix $\mathbf{K}$ and the control law can be defined as:

$$\Delta\mathbf{u} = -\mathbf{R}^{-1}\mathbf{B}^T\mathbf{P}\Delta\mathbf{x} = -\mathbf{K}\mathbf{x} \tag{3.9}$$

With this operation, which does not require high computational time, we have built a Multi-Input Multi-Output control system based on a model of the real system and that is tunable by the user. The procedure is repeated N times, giving a different matrix $\mathbf{K}$ for each wind speed, then the gains are interpolated on-line to also cover the speeds between the chosen trim points.
As the controller is built from a reduced model of the turbine, inaccuracies in the rotor speed tracking may arise due to the model mismatch or non optimal weights, introducing a steady state error on the rotor speed. A solution to this problem is to augment the system with a new state: $\int \Omega dt$. By introducing the integral state the controller follows better the rotor speed set-point it has been given and with less oscillations with respect to the standard LQR control, especially at wind speeds above rated, as can be seen in fig. 3.3.

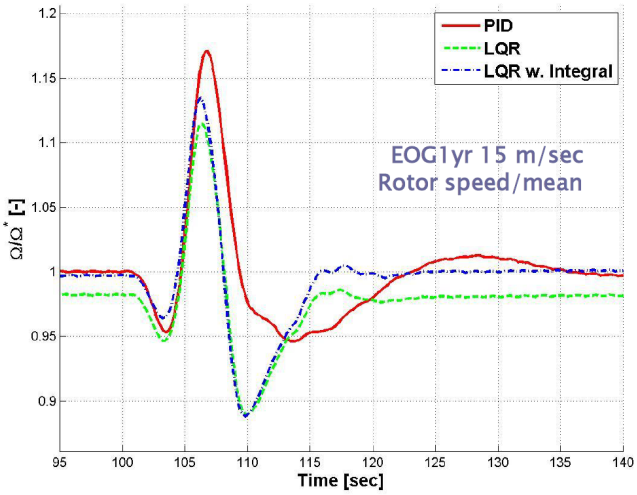

Figure 3.3: *Comparison of rotor speed response to a gust for different control system. In particular, standard LQR shows high steady state error.*

3.2 Cp-lambda

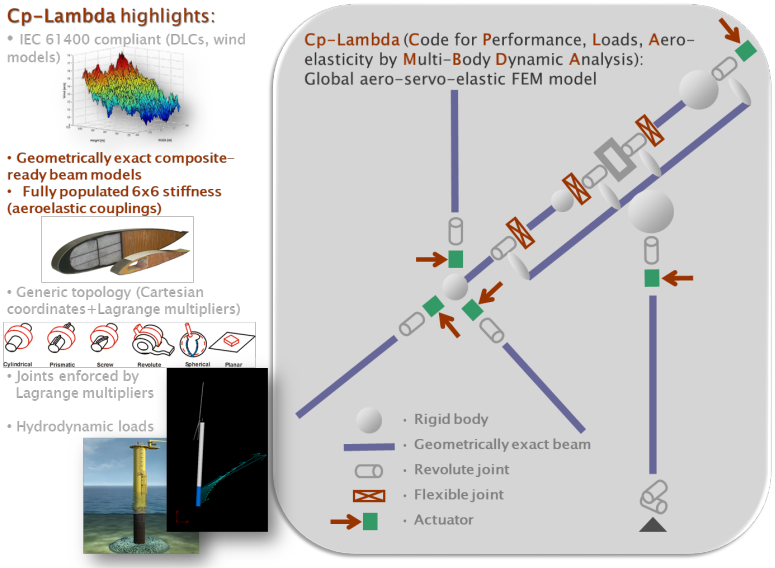

Figure 3.4: *An example of a multi-body model from Cp-Lambda.*

The tool used to perform the aerolastic simulations is called Cp-Lambda [27], a non linear solver using a multi-body finite element method, developed by the

Aerospace department at Politecnico di Milano. Initially developed for helicopter applications, due to his high versatility it has been implemented to perform analysis for wind turbines under standard or extreme operating conditions. It has been validated with both aerolastic codes and through experimental data. By using the multi-body approach, it is possible to build a structure by combining smaller and simpler items from a library, which contains both rigid and flexible elements, such as beams, joints, actuators and sensors with the following properties:

- **Beams**: described by a full 6x6 stiffness matrix, allowing for a complete aerolastic description of the problem. They can be modelled geometrically and it's reference line can be curved or twisted;

- **Joints**: consisting of spring dampers backlashs and friction that can be cylindrical, revolute, spherical etc. They can be rigid or flexible and are enforced by Lagrange multipliers;

- **Actuator**: can be modeled as linear or rotational and can be described with first or second order dynamics;

- **Sensors**: can be used to measure loads, displacements, velocities, angles and more. Some of them provide information to the control system throughout the simulation, like wind speed and rotor speed, while the others can only be visualized by the user for post processing.

The tool uses the blade element momentum theory to model the aerodynamics, allowing to associate a lifting line to each item using a 2D strip theory, with some correction in order to take into account for tip losses, unsteady flow and dynamic stalls. The geometry of the airfoils is not required, but their aerodynamic coefficients are. As for the wind profile, Cp-Lambda builds a grid, centered at the hub and large enough to cover the whole rotor. At each point of the grid must be given a time history of the wind components, for turbulent winds, they have can be generated by using Turbsim [28], which allows to generate a randomized wind grid for different configurations, i.e. normal of extreme turbulence, while gusty winds are automatically produced by the subroutines in the code. Cp-Lambda has a built-in post processor which allows to perform analysis on the results from the simulations, it is able to read the sensors parameters and print their time histories as well as computing the signal's Fourier transforms and PSD for vibration analysis. It's also able to compute the power curve, AEP and CoE of the turbine if a cost model is provided, and ultimate loads, displacements and fatigue by performing a Rainflow analysis as well.

3.3 Main results of the baseline configuration

In this section, the key performance indicators of the baseline turbine without any WFC installed are presented, they will serve as a way to measure the effects of the control strategies under study on the turbine. The simulation have been conducted considering design load cases (DLC's), as listed in table 3.3 so that we could evaluate the behavior of the machine for different operative condition, akin to how wind turbine certification is performed. However, although international guidelines suggest the use of at least six different random seeds for turbulent wind generation and to average the result to validate the model [29], since this is a comparative analysis and not a full certification of the turbine, only one seed has been considered to reduce the total computational time.

Situation	DLC	Wind type	Safety factor	Faults
Power production	1.1	NTM	1.35	No
	1.3	ETM	1.35	No
	1.4	ECD	1.35	No
	1.5	EWS	1.35	No
Power production plus faults	2.2a	NTM	1.1	Freeze on pitch
	2.2b	NTM	1.1	Grid loss
	2.2f	NTM	1.1	Pitch runaway
	2.3b	EOG	1.1	Grid loss
Parked	6.1	EWM	1.1	No
	6.2	EWM	1.1	Grid loss

Table 3.3: *DLC's simulated on the baseline configuration.*

3.3.1 Power production

The power curve obtained by DLC 1.1 is illustrated in Fig.3.5, as can be seen, the LQR controller follows well the nominal power curve even though the turbine has not been designed with such control system in mind, in fact it mostly shows at wind speeds around rated, where because of the unsteady wind speed the operational state goes between partial and full loading conditions. For this configuration, the total Annual Energy Production (AEP) is of 46.1 GWh/yr.

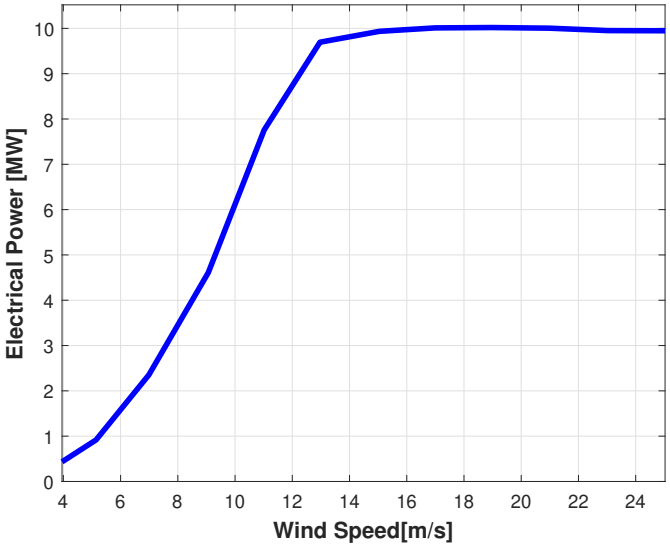

Figure 3.5: *Baseline Power Curve.*

3.3.2 Ultimate loads

To determine whether the turbine can operate safely or not a load envelope analysis must be performed, this time all DLC's have been taken into account to have an extended variety of conditions in which the turbine may operate, in the following paragraphs the maximum loads for different parts of the turbine are presented, including from which DLC they come from to give a better idea of which situation brings the worse loading for each component.
Starting from the blade root, only the greatest value for each load component amongst all three blades have been selected for ultimate load analysis. The values are shown in table 3.4. As can be noted, the maximum flapwise and combined moment are given by DLC 1.3 slightly above rated, probably due to the harsh turbulence adopted in that particular DLC. In fact the same can be seen by looking at the ultimate tip displacements, where one of the blades bends over 13.8m towards the tower.

Type	Value [kNm]	DLC
Flapwise	65920	1.3
Edgewise	38408	1.4
Combined	69073	1.3

Table 3.4: *Blade root ultimate loads.*

While this value is over the maximum allowed, given by 70% of the clearance between blade tip and tower, thus a maximum tip displacement of 12.77m, the blade is considered far enough from the tower during the event to pose a safety threat, in fact the blade is at an azimuth angle of about 270° when the maximum displacement occurs, where common practice during structural design is to consider the value of the maximum deflection only when the blade is in close proximity with the tower.
Although certification is not the main goal of this work, a more accurate analysis has been done on the baseline configuration, this time we plotted the tip displacement as a function of the angular position of each blade with respect to the azimuth. Then we only considered the values of the displacement in the interval of angles ±30° from the tower and registered the maximum value in that range. In this case the maximum tip deflection becomes 12.63m, as shown in table 3.5, which is below the clearance limit required for certification. However, the margin is rather low, being slightly above a tenth of a meter from the limit, highlighting the fact that tip displacement is often an active design constraint in fiber glass blade design.

Value [m]	DLC	Blade
12.63	1.3	2

Table 3.5: *Blade tip ultimate displacement.*

Regarding the tower, bending moments have been recorded for both the base and the top of the structure, giving the corresponding values of Fore-aft., Side-side (as well their combined moment) and torsional ultimate loads that are measured during the simulations.

Sensor	Type	Value [kNm]	DLC
Tower top	Fore-Aft.	74776	1.4
	Side-Side	46239	6.2
	Torsion	62843	1.4
	Combined	75138	1.4
Tower base	Fore-Aft.	576264	2.3b
	Side-Side	381043	6.2
	Torsion	63190	1.4
	Combined	578388	2.3b

Table 3.6: *Tower ultimate loads.*

From table 3.6 can be seen the importance of DLC 1.4 on the tower envelope. And even though for most conditions the Side-side moment is much lower compared to the Fore-aft. moment because normally the rotor is kept perpendicular to the wind, DLC 6.2 simulates a parked condition in extremely turbulent wind for all possible wind directions, clearly when the wind blows parallel to the rotor the Side-Side moment is at his highest, explaining the high value for the bending load. DLC 2.3b makes an appearance on the tower root due to the harsh combination of an extreme gust and grid loss at the same time.
Lastly, the hub ultimate loads are presented below in table 3.7, in this case, together with the moments for Nodding and Yawing, the maximum value for the rotor thrust is measured, given it's importance in the design process.

Type	Value	DLC
Thrust	2844 kN	6.2
Nodding	64600 kNm	1.4
Yawing	58796 kNm	2.2f
Combined	73748 kNm	1.4

Table 3.7: *Hub ultimate loads.*

Similarly to the tower load envelope, DLC 1.4 plays an important role on the ultimate loads, and DLC 2.2f gave the maximum value for the yawing moment, probably due to the imbalance caused by the pitch runaway of one of the blades. Looking at all values, it is clear the impact of DLC's 1.3, 1.4 and 6.2 on the load envelope of the turbine, with many of the main performance indicators of structural design having their maximum value coming from these three cases which represent extreme wind conditions. DLC 2.2f and 2.3b show up too and contribute in defining the envelope, however DLC 1.5, 2.2a and 2.2b are not present in the ultimate loads presented above. To evaluate how these DLC compare with the others, we performed a ranking analysis on ultimate loads, which allows to order all DLC's by the impact they have on a particular sensor. This analysis has been repeated for all of the load types illustrated above, and since DLC 1.5 has a relatively low impact on the loads when compared to other conditions and DLC 2.2f being a strictly worse situation than DLC 2.2a due to the increased danger of the pitch runaway with respect to the pitch freeze, we decided that, moving forward, to exclude the DLC's 1.5 and 2.2a from the set of simulations that will be repeated with the WFC implemented to reduce the total computational burden. For more information about the results of the ranking analysis, see appendix A.

3.3.3 Fatigue loads

Due to the periodic nature of the loads acting on wind turbines, they are particularly prone to fatigue damage. For this reason a fatigue analysis is recommended in order to evaluate the turbine life cycle. To do so we computed the damage equivalent load (DEL), a metric commonly used to evaluate fatigue loads, by running a Rainflow analysis on the sensors' time histories from DLC 1.1, which represents the standard operational conditions during the estimated lifespan of the turbine and according to the certification guidelines [29].
The following plots in figs. 3.6 to 3.8 represent the obtained DEL for different load directions as a function of the wind speed, while table 3.8 contains the cumulated value for each of them, computed by weighting the DEL with the Weibull wave function relative to class 1A wind.

Type	Value [kNm]
Blade Flapwise	29310
Tower top Fore-aft	25709
Tower base Fore-aft	117731
Hub Nodding	25651
Hub Yawing	24326

Table 3.8: *Baseline Cumulated DEL's.*

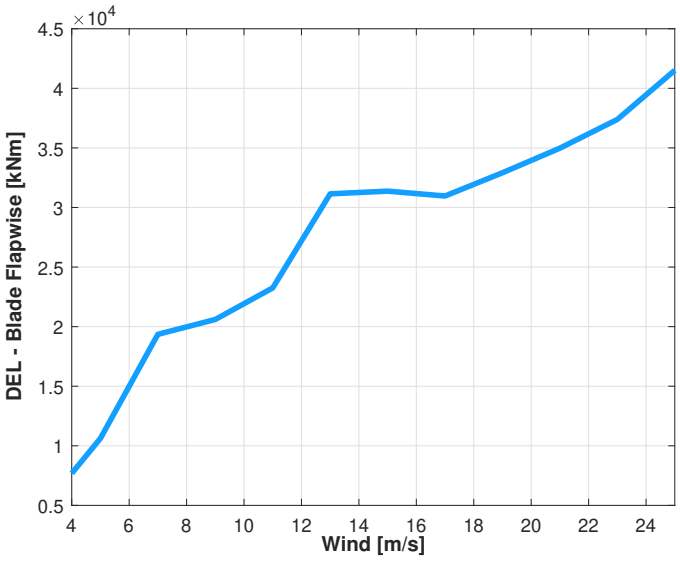

Figure 3.6: *DEL for Blade Flapwise.*

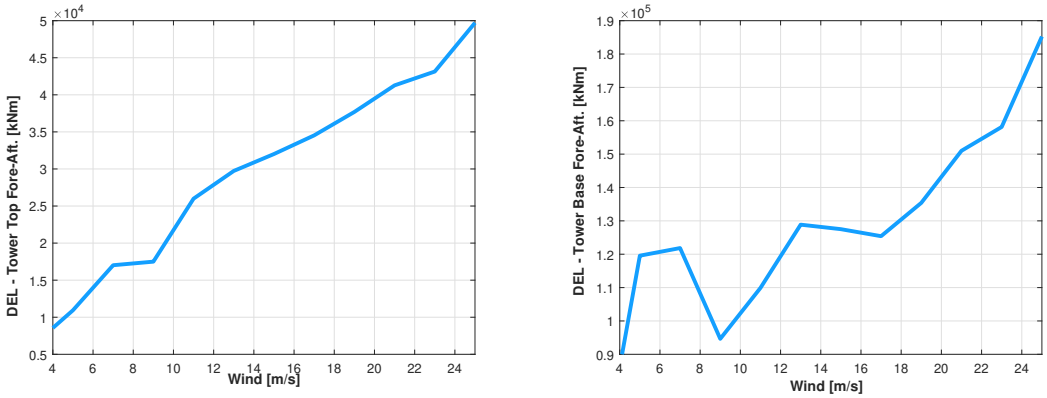

Figure 3.7: *DEL for tower fore-aft. Left plot: tower top. Right plot: tower base.*

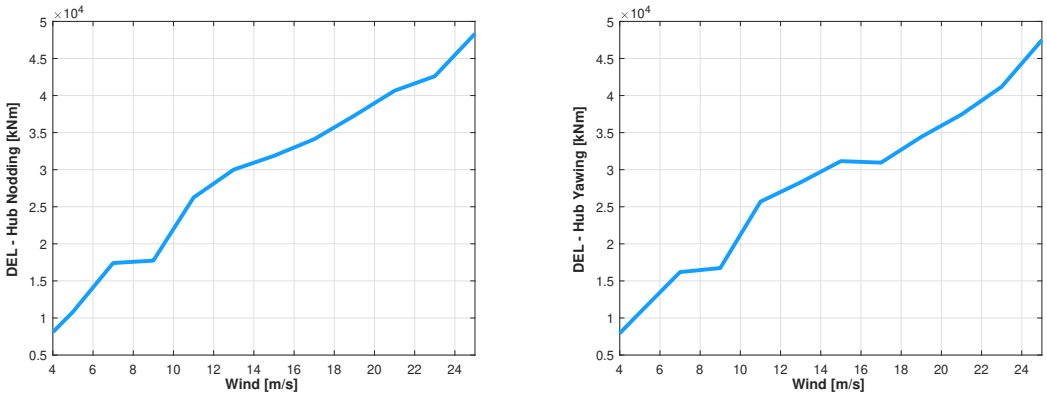

Figure 3.8: *DEL for Hub. Left plot: Nodding moment. Right plot: Yawing moment.*

Chapter 4

Parametric analysis of the effects of different wind farm control configuration on the turbine

In this chapter we carry out a parametric analysis on the reference turbine presented in the previous chapter, installed with both yaw steering and derating, for different possible configurations of the two wind farm control systems. The goal is to investigate how this combination impacts on the turbine's main performance indicators, and weather or not the introduction of derating could lower the increase in loads brought by the yaw-based wind farm control on the operated turbine as initially hypothesized. Given that there are no defined standards which rule wind farm design, we decided to carry out the study following international guidelines for individual turbines, as has been done in chapter 3, such that the comparison is as realist as possible. In this regard, we considered the list of DLC's from table 4.1:

Situation	**DLC**	**Wind type**	**Safety factor**	**Faults**
Power production	1.1	NTM	1.35	No
	1.3	ETM	1.35	No
	1.4	ECD	1.35	No
Power production plus faults	2.2b	NTM	1.1	Grid loss
	2.2f	NTM	1.1	Pitch runaway
	2.3b	EOG	1.1	Grid loss

Table 4.1: *DLC's simulated for the parametric analysis.*

As can be noted, the DLC's are the same as the study on the baseline configuration, save for the ones that have been considered not relevant for this analysis

due to their lower impact on the loads, as explained in the previous chapter. Also DLC 6.1 and 6.2 are missing here, since both of them have the turbine in parked configuration hence the control system is off, as well as the hypothetical wind farm control, therefore the resulting loads would be identical to the baseline simulation. However it is important to note that they are still relevant in the computation of the load envelope for all the investigated configurations, but they have been simulated only once to save time.

4.1 Implementation of the wind farm control

In this section we give a brief explanation of how the WFC techniques have been implemented in the simulation environment, as well as introducing the values tested for each of them.

4.1.1 Yaw misalignment

For yaw-steering control, the turbine have been rotated by the set of yaw angles θ = [-25° -15° 0° 15° 25°] with respect to the main direction of the wind, where positive angle meas a counterclockwise rotation. The turbine is slowly rotated from the reference position at the start of each simulation during the transient period to ensure continuity on the sensors measurement. By imposing an angle the yaw control system, the one responsible to keep the hub perpendicular to the wind, is turned off to ensure that the angle of the rotor from the north direction is constant during turbulent simulations, ignoring eventual wind direction changes.

4.1.2 Derating

For derating, the optimal power coefficient computed by the Cp-Lambda code has been reduced by the set of factors $\mathbf{n}$ = [0 2.5% 5% 10% 15%]. For this study, we decided to maintain the tip speed ratio constant at the optimal value in both partial (for instance, strategy n. 3 from fig. 2.2) and full loading. To compute the new reference conditions for each wind speed, the routine finds the optimal regulation parameters from the C_p vs TSR vs Pitch curve calculated beforehand, then reduces the power coefficient by the desired amount and uses the result together with the optimal TSR to get the new value for the pitch angle from the curve, as well the adequate value for the generator torque to maintain the power constant in region 3. An example of the difference in regulation is illustrated in fig. 4.1.
Once the new reference control values have been obtained, the new gains of the LQR controller are computed. While the values of the weights have been maintained the same for all configurations, every one of them will have a slightly dif-

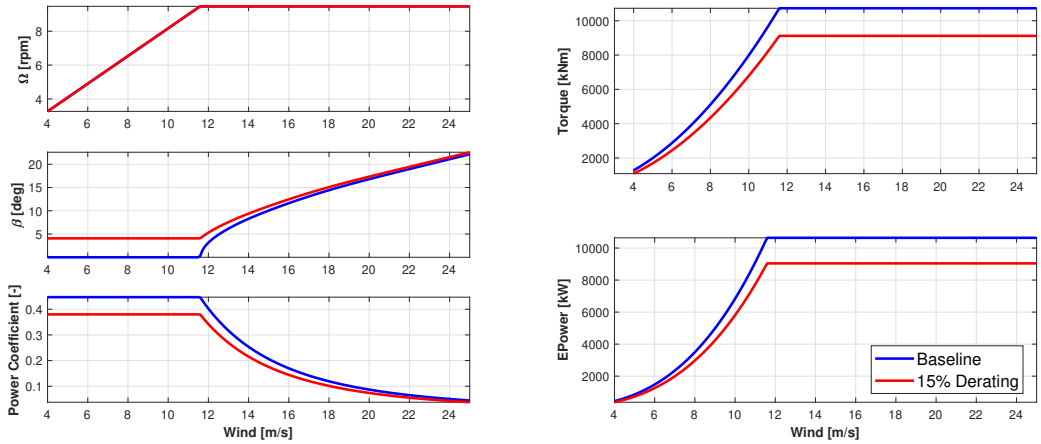

Figure 4.1: *Difference in reference values from the application of 15% derating.*

ferent controller operating the turbine because of different trim values, opening the topic for a more in-depth optimization for each derating percentage. This optimization, however, has not been performed as is not the main scope of this work.

4.1.3 Combination of the strategies

The two sets of values are then put together to cover all different combinations, for a total of 25 sets of simulation. By how both strategies have been implemented, and how Cp-Lambda handles the control system, they merge seamlessly. For each of them we ran the aerolastic simulations representing the DLC's in table 4.1 above. Then all the results have been post processed to identify how the key performance indicators vary with different configurations.

4.2 Key performance Indicators

In this section we present the main results from the parametric analysis in terms of the turbine KPI and how they are effected by the implementation of the WFC and for different setup combination. In particular, the values relative to power production, ultimate loads, displacement and fatigue will be shown both as their absolute values and the percentage change with respect to the baseline condition presented in Chapter 3.

4.2.1 Power Production

The main purpose of a wind turbine is producing electrical power, and while the premise of WFC is to increase the wind farm efficiency, it is at the expense of the operated turbine. To measure the impact of the control on the production of the operated machine, we computed the power curves from each configuration by post-processing the data coming from DLC1.1 which is the normal operative condition of the turbine, following the procedure defined by IEC [29].
A fundamental performance indicator is the AEP, the comparison is presented in fig. 4.2, confirming that both strategies are detrimental for the power generation of the single turbine.

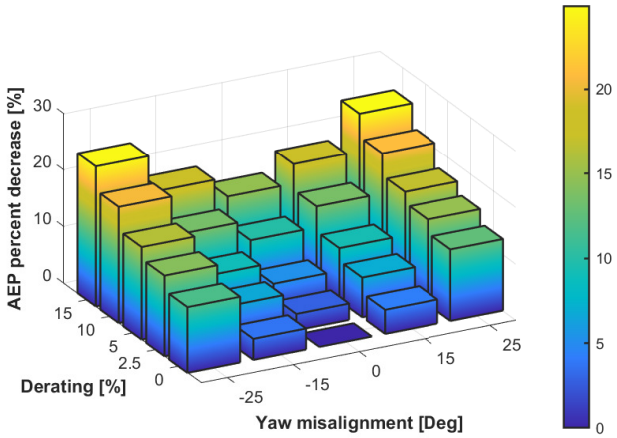

Figure 4.2: *AEP percent decrease.*

Then, fig. 4.3 shows a comparison for all power curves. The effect of derating is noticeable, a 10% derating corresponds to roughly an equivalent reduction in production for all wind speeds, indicating that the strategy has been implemented correctly. The impact of the imposed yaw angle is more subtle, but it is visible at speeds below rated, while for high wind speeds the loss in power production is almost zero. This is as expected, in fact, from a physical point of view, since the rotor is not perpendicular to the wind the speed component that is responsible for the power production is the one orthogonal to the rotor disk. As a consequence, the wind speed that is seen by the rotor is $Vcos(\theta)$, and since the power produced is proportional to the cube of the wind speed, even a small yaw angle can have a great impact on the energy generation. Instead, when $Vcos(\theta) > V_{rated}$ the turbine goes in full loading configuration and keeps the power constant at the designed value regardless of the misalignment.

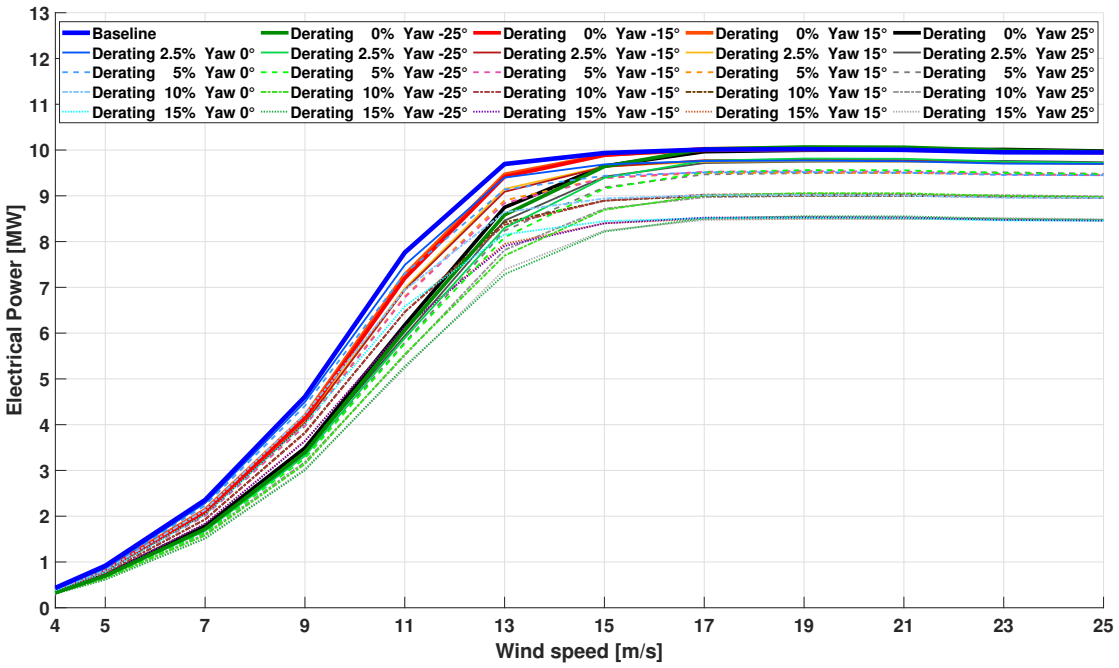

Figure 4.3: *Power curve comparison.*

4.2.2 Ultimate loads

Following power production, ultimate loads are of paramount importance in wind turbine design, as they are often active constraints during the design process. In the following pages we present the results of the parametric analysis, showing the effect of the two wind farm control laws on the load envelope of the turbine with respect to the condition without WFC.
The data will be presented in the following way: since all DLC's of table 4.1, plus the ones in parked condition, have been taken into account for the load envelope evaluation, it may be also interesting to show the ones responsible for each kind of ultimate load in each configuration. To do so we decided to show the raw values in table form with each cell colored depending on which DLC they come from. A legend on the colors adopted is in table 4.2:

ETM (DLC 1.3)
Gust (DLC1.4)
Failure (DLC 2.2b, 2.2f, 2.3b)
Parked (DLC 6.1, 6.2)

Table 4.2: *DLC color legend.*

Then a bar plot where all values will be scaled with respect to the baseline configuration, thus showing the percentage increment (or reduction) for each configuration to simply determine at a glance whether the value increases or decreases.

Blade

Firstly, the ultimate loads for the blade root are represented in figs. 4.4 to 4.6, showing the variation in the flapwise, edgwise and combined direction. From fig. 4.4 there is a noticeable increase in the flapwise direction (and consequently, combined) due to the Yaw misalignment, with an increase of about 20% at -25°. As expected the introduction of this WFC law brings an increase in loads. However, when paired with derating, the maximum load is greatly reduced even for low percentages of the latter.
Figure 4.7 shows the variation in maximum tip deflection recorded in proximity to the tower, as has been done in section 3.3.2 for the baseline configuration. While the danger brought by the imposed yaw angle is noticeable, which would require a blade redesign in order to reduce the deflection if it would be implemented alone, it is also striking the effect of the derating even at low percentages, this might be due to the increased pitch angle used to impose the axial induction control, which helps braking the rotor. Also, as can be seen in table 4.6 the failure happening in DLC 2.2f becomes more prevalent for higher derating percentages, this might be caused by the pitch runaway failure, where the pitch control of one blade has a malfunction which rapidly lowers the pitch angle up to 0 degrees. Therefore, the failure has great impact on the blade regardless of the increased initial pitch angle. Moreover, considering the price on the power production, percentages above 10% don't seem convenient. On the contrary low percentages are enough to keep the displacement below or near the baseline values with little impact on the power production.
Since the results from this analysis are as hypothesized and the two WFC strategies can complement each others, at least regarding the load envelope of the blade, and most importantly the tip deflection which is more often than not the most important constraint in fiber glass blade design, it might be thoughtful to investigate what happens along the blade span in terms of ultimate loads. Therefore, fig. 4.8 reports the variation in ultimate combined moment recorded at the maximum chord position. As can be noted, the general trend with respect to yaw misalignment and derating is similar to the previous results on the base and tip of the blade, confirming once again the effectiveness of the combined wind farm control.

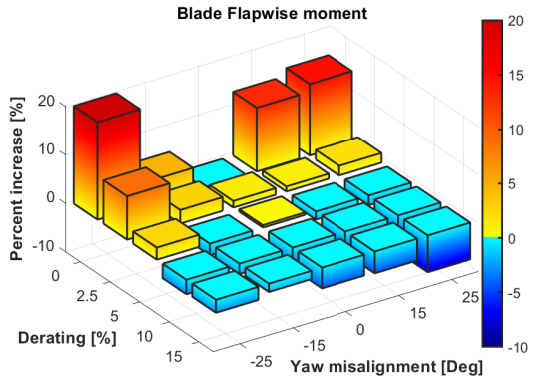

Derating [%] \ Yaw angle [Deg]	-25	-15	0	15	25
0	79.2	69.0	65.9	74.6	75.6
2.5	71.8	67.8	66.8	66.6	67.2
5	67.6	64.3	66.2	64.8	64.6
10	63.9	64.5	63.0	62.7	60.9
15	64.1	64.8	63.0	62.9	60.9

Figure 4.4 & Table 4.3: *Blade root flapwise ultimate load comparison (in MNm).*

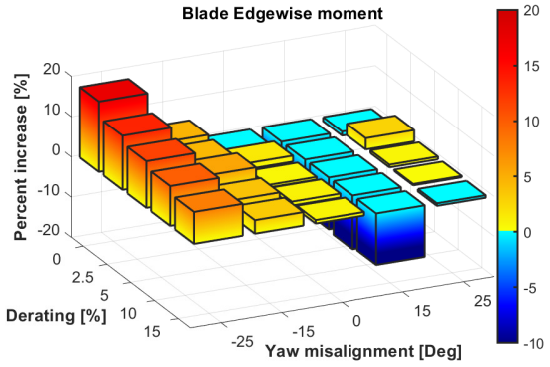

Derating [%] \ Yaw angle [Deg]	-25	-15	0	15	25
0	45.1	40.2	38.4	36.3	38.0
2.5	43.6	40.1	39.0	36.0	39.5
5	42.9	40.5	38.7	33.5	38.7
10	42.2	39.9	38.8	33.3	38.5
15	41.5	39.7	38.7	33.5	38.2

Figure 4.5 & Table 4.4: *Blade root edgewise ultimate load comparison (in MNm).*

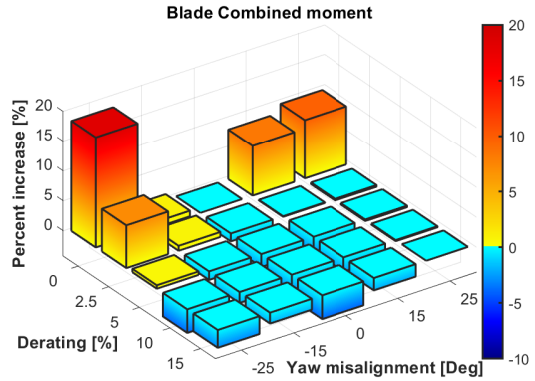

Derating [%] \ Yaw angle [Deg]	-25	-15	0	15	25
0	81.8	69.7	69.1	74.8	75.8
2.5	74.0	69.6	68.2	69.0	68.9
5	69.5	68.1	67.6	67.2	68.9
10	66.4	67.8	66.2	67.4	69.0
15	67.0	67.8	66.3	67.6	69.1

Figure 4.6 & Table 4.5: *Blade root combined ultimate load comparison (in MNm).*

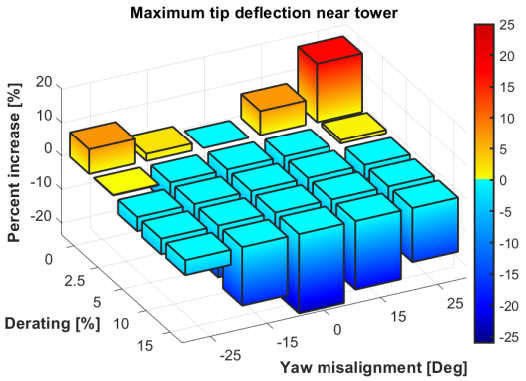

Derating [%] \ Yaw misalignment [deg]	-25	-15	0	15	25
0	13.56	12.90	12.63	13.54	14.83
2.5	12.65	11.74	11.17	11.85	12.76
5	12.10	10.95	11.04	11.07	12.09
10	12.04	10.69	10.17	10.28	11.22
15	12.07	10.44	9.66	10.06	10.60

Figure 4.7 & Table 4.6: *Blade tip ultimate deflection comparison (in m).*

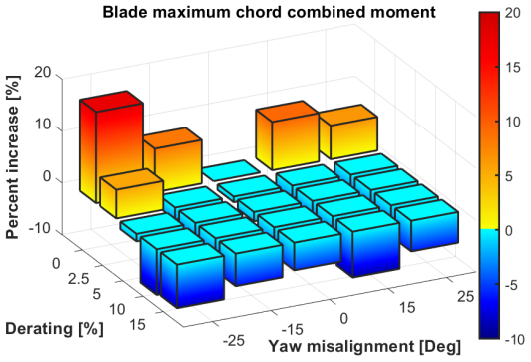

Derating [%] \ Yaw angle [Deg]	-25	-15	0	15	25
0	40.4	37.7	37.0	38.0	38.3
2,5	36.3	36.5	37.1	38.1	38.5
5	35.5	36.6	37.0	38.1	38.5
10	35.5	36.6	37.0	38.1	38.5
15	35.6	36.8	37.3	38.4	38.7

Figure 4.8 & Table 4.7: *Blade combined ultimate load at maximum chord comparison (in MNm).*

Following these results, since the main goal of this project is to evaluate whether the combinations of the two WFC laws is able to maintain the values of ultimate loads and tip deflection equal to the configuration without neither of the two, and if so, for which combinations, we evaluated how much derating has to be implemented in function of the yaw misalignment. To do so, we linearly interpolated the results and found the intersection with the baseline's value for each yaw angle. In this way, we can evaluate the theoretical power reduction needed for a particular misalignment from the simulation's data.
Figure 4.9 represents the results for ultimate tip deflection and blade root combined load, showing that low values of derating are enough to maintain these parameters equal to the baseline, especially for tip displacement. As expected, higher misalignments demand higher compensations, with tip deflection suggesting a parabolic relation between the two control strategies. For the combined load, instead, the derating required is higher, with the only exception at 25°, where 2.5% is enough to balance the increase in ultimate load (fig. 4.6). Also, the behavior is different with respect to displacements, even if we exclude the rightmost point in the graph, this time the relation is almost linear with respect to the absolute value of the angle.

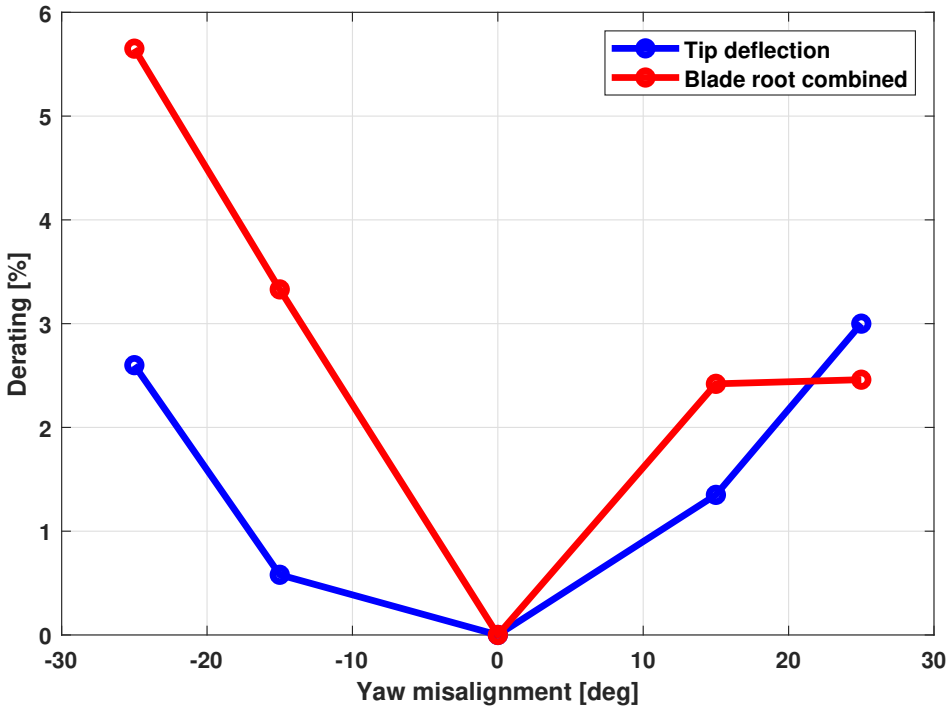

Figure 4.9: *Derating needed to balance the effect of misalignment in function of the yaw angle. Blue line: maximum tip deflection. Red line: blade root combined ultimate load.*

Tower

The ultimate loads for both top and bottom of the tower have been recorded and presented in figs. 4.10 to 4.13 and tables 4.8 to 4.11. In this case, along with torsion, only the fore-aft./side-side combined ultimate loads for both sensors is reported, this is due to two reasons: firstly, it represents the direction of maximum bending which, generally, is not either of the sensors and because of the cylindrical shape of the tower no direction is favorite, unlike for the blade. Secondly, the tower sensors do not rotate with the rotor, making the comparison of individual Fore-aft. or Side-side between different yaw angle not possible.
Again, the introduction of derating has a positive effect on the combined bending moment, especially for the tower base, but not as prominent as in the blade case. In fact, the values tested are not enough to balance the negative effects of wake redirection, which brings a substantial increase in most situations, especially for tower top combined, where the increment is over 30% with 25° of misalignment. This might be dangerous and requires additional care if the WFC is installed on already existing turbines. Also, the axial induction seems to have little to no impact on the torsional moment, while it clearly increases in the majority of simulations that use the yaw-based WFC due to the rotor not being perpendicular to the wind anymore.
In this case, DLC 1.4, 2.2f and 2.3b play a key role on the tower load envelope, which is not surprising since they were already responsible for the tower's ultimate loads in the baseline configuration.

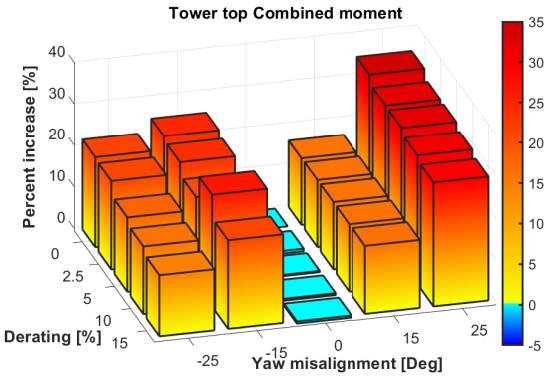

Derating [%] \ **Yaw angle [Deg]**

	-25	-15	0	15	25
0	91.4	93.9	75.1	87.2	101.0
2,5	91.1	93.2	74.7	87.2	99.4
5	88.5	90.9	74.9	87.3	99.4
10	87.3	95.3	74.8	87.3	98.4
15	86.1	91.1	74.7	87.4	97.5

Figure 4.10 & Table 4.8: *Tower top combined ultimate load comparison (in MNm).*

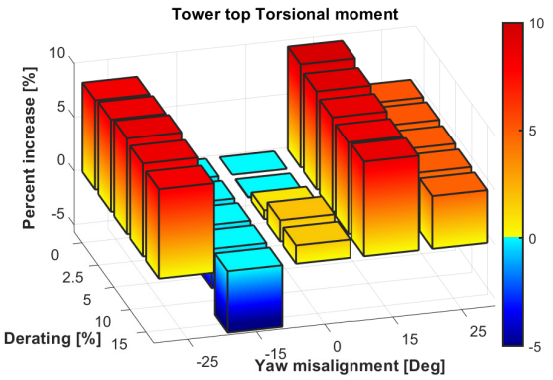

Derating [%] \ Yaw angle [Deg]	-25	-15	0	15	25
0	68.1	62.3	62.8	68.9	66.2
2,5	68.2	62.0	62.8	68.6	66.1
5	68.4	61.8	63.4	68.4	66.0
10	68.3	60.6	64.1	68.2	66.0
15	68.0	59.3	63.9	68.4	65.9

Figure 4.11 & Table 4.9: *Tower top torsion ultimate load comparison (in MNm).*

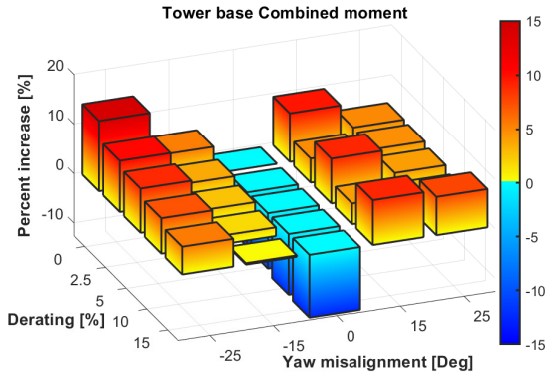

Derating [%] \ Yaw angle [Deg]	-25	-15	0	15	25
0	661	610	578	635	607
2,5	638	600	515	607	606
5	630	594	514	631	603
10	620	589	507	603	597
15	611	580	505	631	623

Figure 4.12 & Table 4.10: *Tower base combined ultimate load comparison (in MNm).*

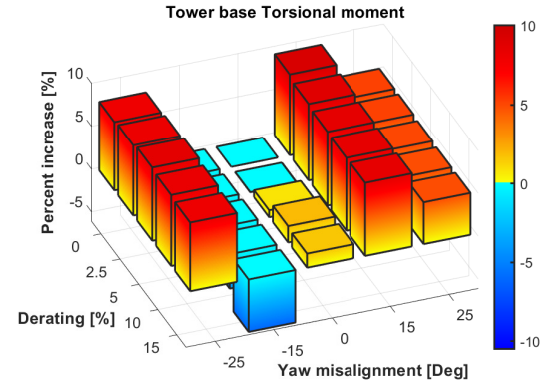

Derating [%] \ Yaw angle [Deg]	-25	-15	0	15	25
0	68.2	62.4	63.2	69.1	66.5
2,5	68.4	62.1	63.2	68.8	66.5
5	68.6	61.9	63.7	68.6	66.4
10	68.4	60.7	64.4	68.6	66.3
15	68.3	59.3	64.2	68.6	66.3

Figure 4.13 & Table 4.11: *Tower base torsion ultimate load comparison (in MNm).*

Hub

The effects of the two strategies of the on the ultimate loads for Thrust, Nodding, Yawing and combined moment acting on the hub are represented in figs. 4.14 to 4.17 and tables 4.12 to 4.15.
Because of his importance in turbine design, we decided to include the thrust force in this analysis, but since it's maximum value comes from DLC 6.2 for all configurations, it is not affected by the WFC.
Regarding the ultimate loads for moments, the results in terms of percentage variation are comparable to the ones for the tower ultimate loads, hence we can draw similar conclusions. The analysis shows again the potential danger of operating the wake redirection WFC, especially for high yaw angles. But while the introduction of derating was able to counter these effects when looking at the blade and, with much lower impact, at the tower, this is no longer true for the hub. In fact axial induction control has no meaningful effect on the hub ultimate loads, even bringing an increase in some cases like at -25° and -15° in fig. 4.15 for example, which is not what was initially hypothesized, and proving its ineffectiveness on the hub envelope. Moreover, the nodding ultimate load experiences a significant increase of over 40% at 25 deg., making the implementation of both WFC strategies not feasible or at least at high wake steering setups.
Speaking of DLC's, apart from thrust which has been already covered, the hub envelope is defined only by DLC 1.4 and 2.2f, the same that were found in the baseline configuration in table 3.7.

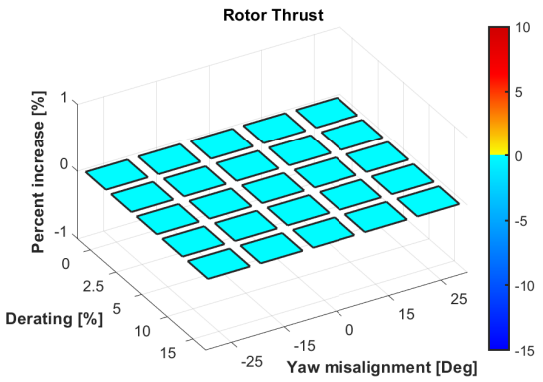

Derating [%] \ Yaw angle [Deg]	-25	-15	0	15	25
0	2.84	2.84	2.84	2.84	2.84
2,5	2.84	2.84	2.84	2.84	2.84
5	2.84	2.84	2.84	2.84	2.84
10	2.84	2.84	2.84	2.84	2.84
15	2.84	2.84	2.84	2.84	2.84

Figure 4.14 & Table 4.12: *Hub thrust ultimate load comparison (in MN).*

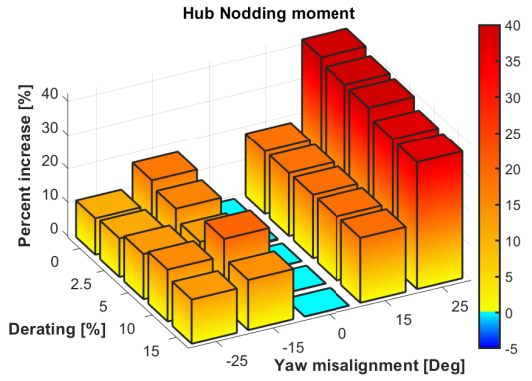

Derating [%] \ Yaw angle [Deg]	-25	-15	0	15	25
0	71.5	76.2	64.6	76.6	91.9
2,5	72.0	75.0	64.4	76.7	90.9
5	73.2	72.9	64.5	76.7	90.8
10	74.5	77.7	64.6	76.8	89.1
15	73.0	74.2	64.6	77.0	88.9

Figure 4.15 & Table 4.13: *Hub nodding ultimate load comparison (in MNm).*

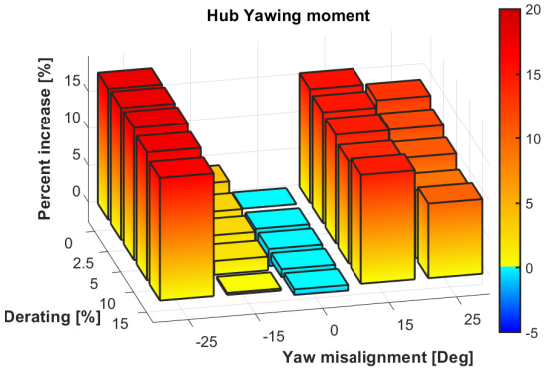

Derating [%] \ Yaw angle [Deg]	-25	-15	0	15	25
0	69.2	61.0	58.8	67.8	66.5
2,5	69.3	60.4	57.3	67.6	65.8
5	69.3	60.2	57.4	67.4	65.1
10	68.9	59.9	58.2	66.9	64.2
15	68.5	59.0	58.4	67.4	64.7

Figure 4.16 & Table 4.14: *Hub yawing ultimate load comparison (in MNm).*

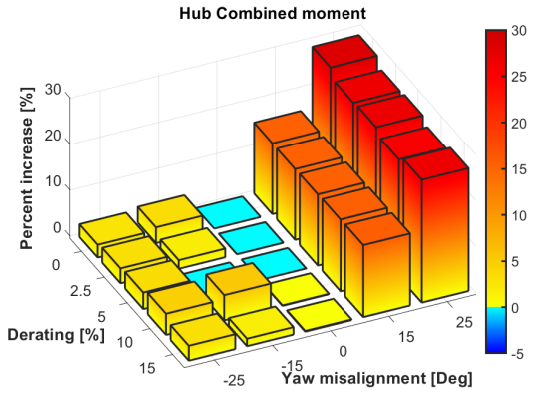

Derating [%] \ Yaw angle [Deg]	-25	-15	0	15	25
0	75.8	76.3	73.7	85.1	94.8
2,5	76.1	75.1	73.8	85.1	93.4
5	76.4	73.4	73.7	85.2	93.6
10	77.1	77.8	73.8	85.3	92.6
15	76.1	74.9	73.9	85.3	93.5

Figure 4.17 & Table 4.15: *Hub combined ultimate load comparison (in MNm).*

4.2.3 Fatigue loads

The last important topic to cover is the effect of the WFC on the deterioration of the machine. Fatigue loads are fundamental to evaluate the lifetime of each component of the wind turbine. In the following paragraphs we compare the results from the Rainflow analyses on the sensor's readings from DLC 1.1 of each configuration. The DEL data will be presented with respect to the wind speed, as well the cumulated values computed by weighting the speed-by-speed DEL's with the Weibull wave function relative to class 1A.
But while for ultimate loads it is enough to measure bending by taking the orthogonal components given by the sensors and summing the two vectors to get the combined value, for fatigue damage this is no longer true. In fact, for the most accurate fatigue evaluation one must find the most heavily loaded direction, which generally is not either of the two sensors, especially when considering a situation in which the rotor is not perpendicular to the wind.Therefore, to find the worst direction, a load rose may be necessary. However, since this procedure is time consuming, as it must be repeated for each configuration, and its implementation is outside the scope of this project, different approaches have been taken depending on the sensors.

Blade

For blade root, the sensors are already rotated according to the rotor, thus we assumed that the comparison is reasonable even for different yaw angles. Figures 4.18, 4.20 and 4.21 represents the results of the Rainflow analysis for Blade Flapwise and Edgewise directions. The former shows an increase in cumulated DEL for negative misalignment but a decrease for positive yaw. In fact by looking at fig. 4.20 for high wind speeds, positive yaw configurations are below the baseline while negative ones gave higher loads at those speeds. Also, derating does not effect the DEL's for fast wind more than a negligible increase. However around rated wind speed derating has a positive effect by lowering the fatigue loads. Similar conclusions can be drawn for the edgewise direction, although the percentile variation is much lower with respect to the flapwise fatigue.
If blade deterioration is a concern, it might be wise to deactivate the WFC for winds above a given speed, for example $15m/s$. When the wind speed is well above the rated value, the flow total energy increases while the extraction done by the turbine is kept constant, therefore the resulting wake has more energy that can be harvested by the downwind turbine, making the effect of the WFC less prominent at fast winds. By doing so the effects of yaw steering on fatigue loads at high wind speeds are avoided. The Rainflow analysis has been performed again,

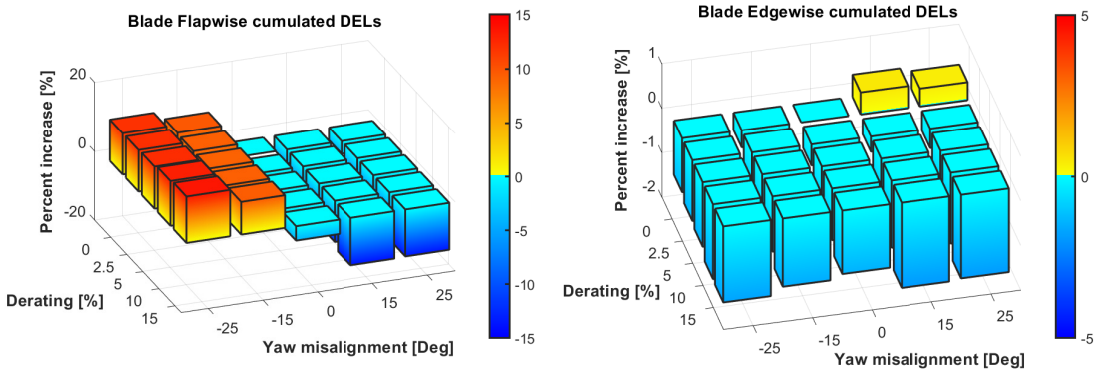

Figure 4.18: *DEL comparison. Left plot: blade root flapwise. Right plot: blade root edgewise.*

this time with the WFC turned off after $15m/s$. The difference is clearly visible in fig. 4.19, especially for the flapwise direction, indicating how much of an impact the yaw misalignment had on the DEL's for high wind speeds and, by consequence, on the cumulated values. Moreover, this time most configuration show a decrease with respect to the baseline results. although the variation is relatively small for all of them. The positive effect of derating is still present, resulting in a small reduction in cumulated DEL proportional to the percentile reserve. In the edgewise direction instead, the results are more similar to the previous analysis, showing the same overall trend.

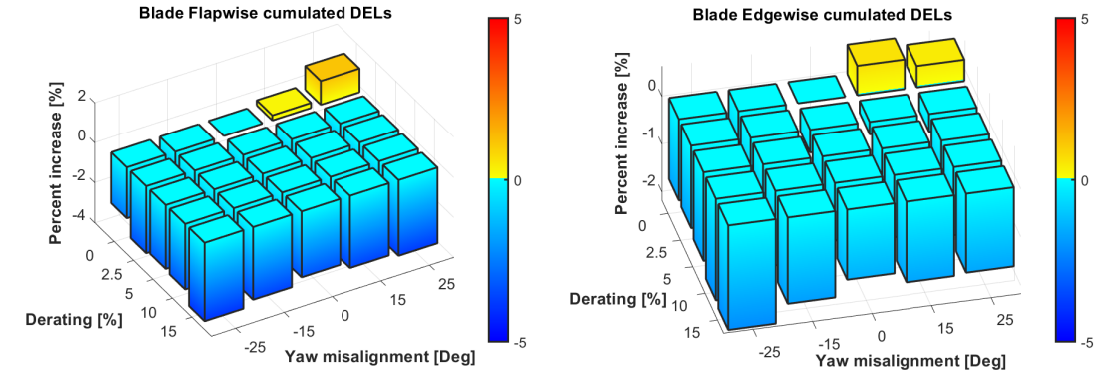

Figure 4.19: *DEL comparison with WFC off at wind speeds above* $15m/s$*. Left plot: blade root flapwise. Right plot: blade root edgewise*

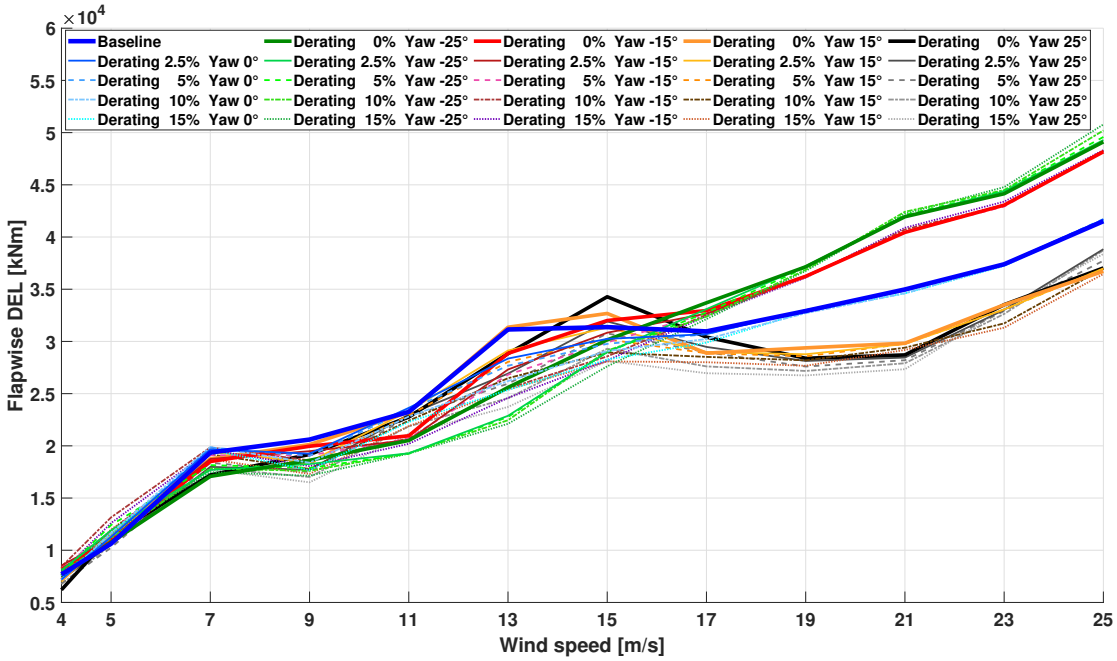

Figure 4.20: *Blade Flapwise DEL comparison wrt. wind speed.*

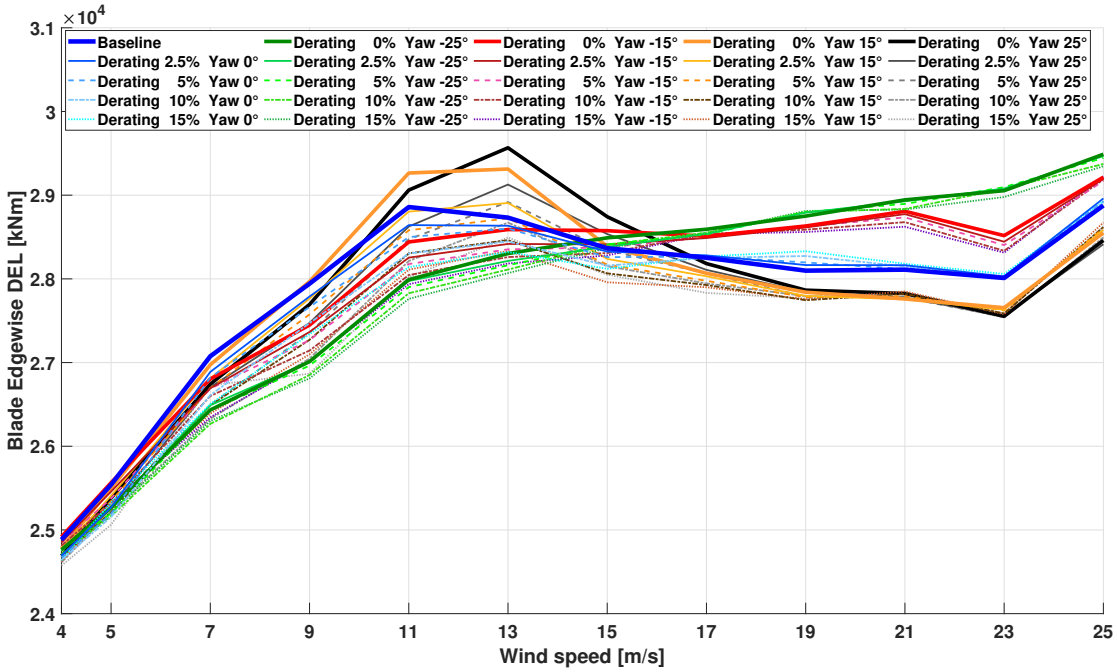

Figure 4.21: *Blade Edgewise DEL comparison wrt. wind speed.*

Tower

Regarding tower base, because the sensor installed does not rotate with the rotor, it would be erroneous to compare the fore-aft. or side-side directions for different yaw angles. From [8] the worst fatigue direction is in accord with the angle of the misalignment, so before running the Rainflow analysis we rotated the time histories of the tower base sensors by the same degree of the yaw misalignment. The results in figs. 4.22 and 4.24 show the comparison. This time, derating has a detrimental effect on fatigue for very low wind speeds but a positive one after $9m/s$, in particular for speeds slightly above rated where the reduction in fatigue loads is remarkable in most cases. Wake redirection on the other hand gave mixed results, showing increases for some combination of wind speeds and angles and decreases for other, which could be connected to the initial assumption on the worst direction. However the increase recorded at 15° is rather small, while in most cases the cumulated DEL are lower compared to the baseline, demonstrating the effect of derating on fatigue.

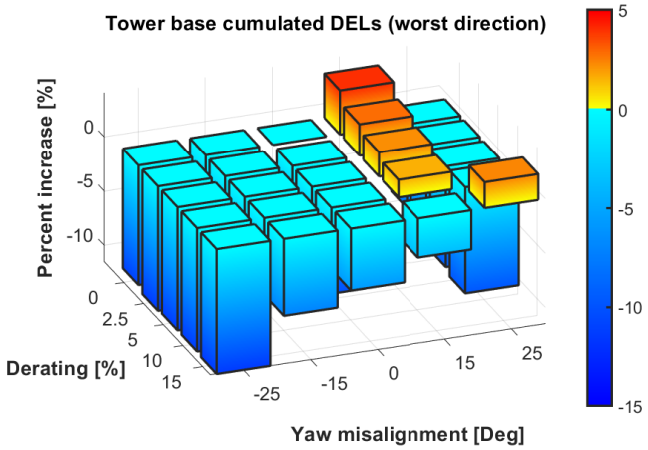

Figure 4.22: *DEL comparison for tower base along the worst direction.*

Hub

The reference frame of the Hub sensor rotate together with the rotor, so we opted to keep the measures as they are provided. The DEL's for Nodding and Yawing are illustrated in figs. 4.23, 4.25 and 4.26. As can be seen, the impact of the two strategies is similar for both direction and relatively small in most cases. Surprisingly increasing the derating percentage generally has a negative effect on the cumulated DEL's across all speeds, especially around rated wind speed, where

the Weibull function is at its peak. On the contrary the misalignment decreases the cumulated fatigue loads up to 4%, which was not expected given the significant increase in ultimate loads for both of them from the previous analysis.

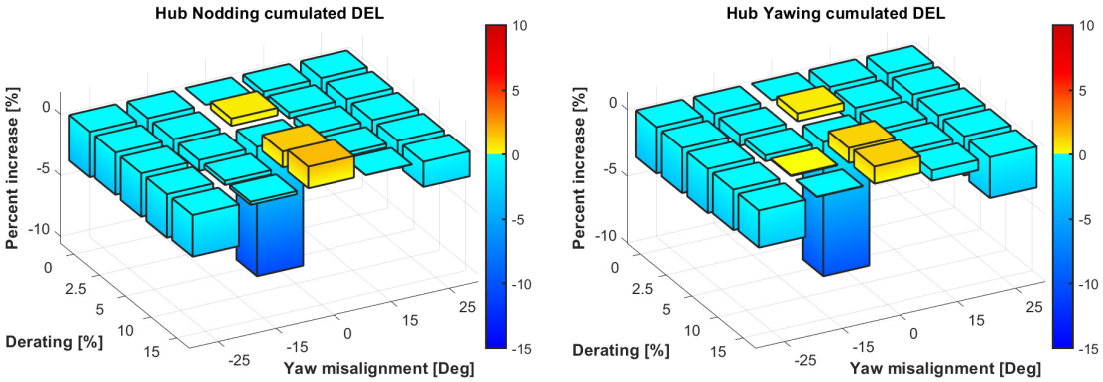

Figure 4.23: *DEL comparison. Left plot: Hub Nodding. Right plot: Hub Yawing.*

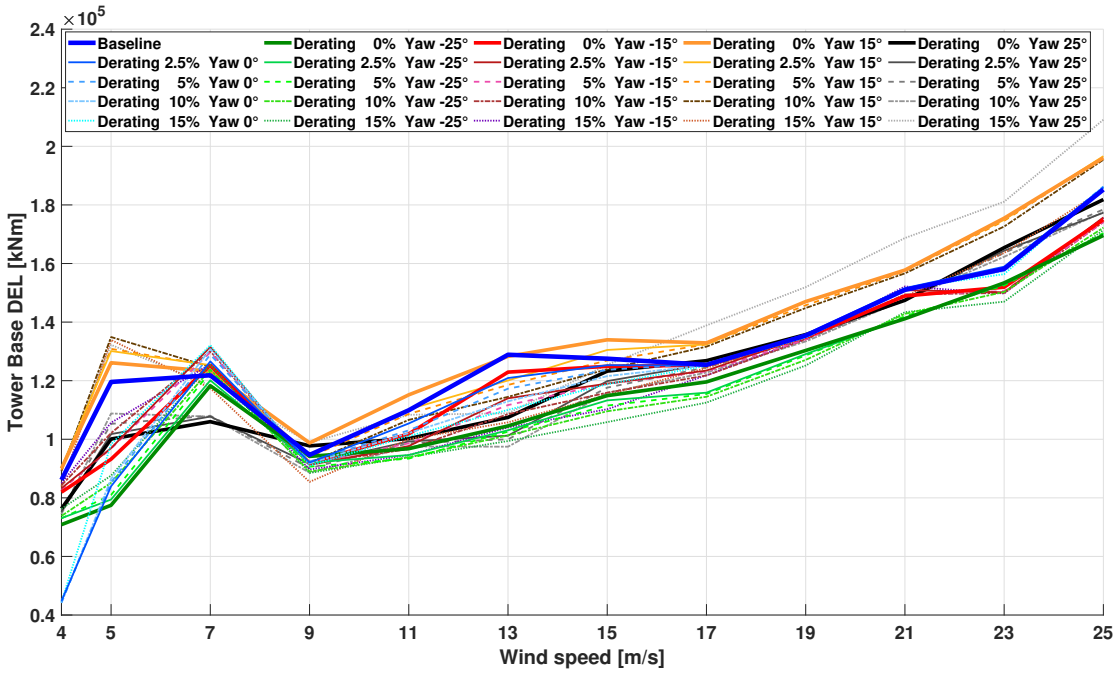

Figure 4.24: *Tower base DEL comparison wrt. wind speed (worst direction).*

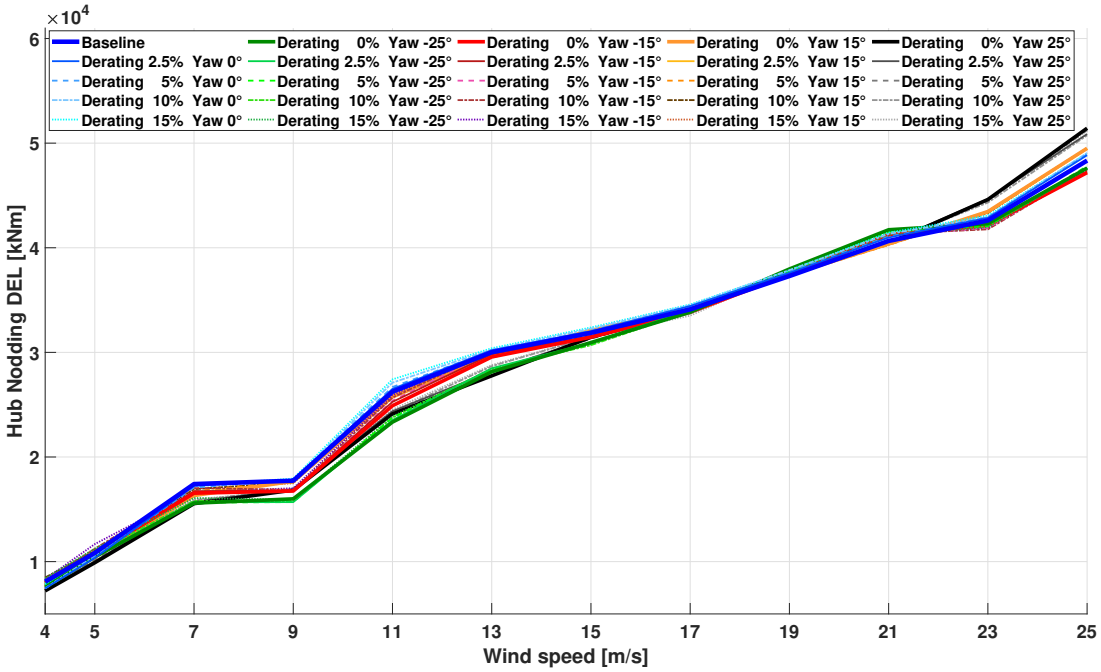

Figure 4.25: *Hub Nodding DEL comparison wrt. wind speed.*

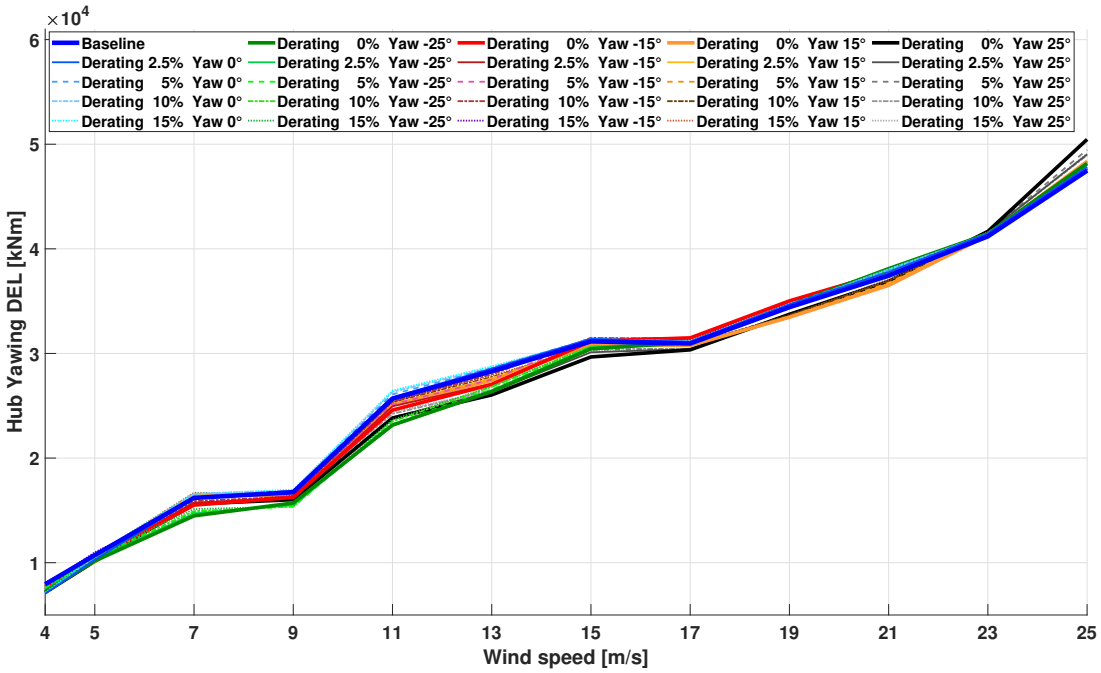

Figure 4.26: *Hub Yawing DEL comparison wrt. wind speed.*

4.3 Main outcomes

Power production shows the expected reductions when the WFC is implemented, however the main reason of its implementation is to gain more than it's lost from the operated turbine by the theoretical increase in production of the downstream turbines. However such analysis is not the scope of the Thesis.
Regarding ultimate loads, the addition of axial induction control alongside the yaw-based WFC is able to balance the drawbacks brought by the latter on the blade load envelope and, most importantly, tip displacement even for small derating percentages. For tower and hub, instead, the impact of derating is less noticeable (and in some cases, not present) and is not able to counter the detrimental effect of Wake steering, requiring additional care in whether these control laws can be implemented or not on already existing turbines and the maximum yaw angle that can be imposed.
From this analysis it is also important to note the prevalence of DLC 1.4 and 2.2f on most configurations. In fact, these two DLC's are responsible for the majority of the ultimate loads. This is not surprising since both cases are already quite demanding on normal turbines and their situations are aggravated by the WFC.
For fatigue loads, no substantial change has been recorded that could impact the turbine life-cycle, considering that the WFC would be active only for some wind directions, with a reduced impact over the life of the machine. But since this analysis would require a statistical study on possible wind directions and is site dependant, it is not included in this project. However, if fatigue damage is a concern, derating could be implemented alone in small percentages to extend the lifetime of a turbine, with a negligible impact on the overall wind farm power production.

Chapter 5

Conclusions and future developments

The aim of this Thesis project was to investigate the effect of axial induction control combined with yaw-based wind farm controllers on the upwind turbine's key performance indicators, mainly the load envelope and fatigue damage. To do so, we performed a parametric analysis with different WFC setups on the INNWIND.EU 10 MW wind turbine by employing mathematical models and aero-servo-elastic solver which represent the state of the art in wind turbine design. For the analyses, we followed certification guidelines for single turbines, since rules regarding wind farm design have not been defined yet.
Firstly, an initial analysis has been carried out on the reference turbine without WFC and equipped with the Poliwind Linear Quadratic Regulator, to provide a benchmark configuration serving as a comparison for the different configuration. Following that, we implemented the two WFC strategies on the baseline model and studied their effect on the turbine for different design load cases. The main outcomes of the analyses are briefly listed below:

- The introduction of a yaw misalignment resulted in an increase in ultimate loads on the blade root, hub and tower, registering an increase of about 40% for some cases.
- The addition of derating has a positive effect on the load envelope of the turbine, especially on the blade root, where even for small percentages is capable of balancing the negative effects brought by the other strategy. The same cannot be said for tower and hub, even though most cases show a small decrease in ultimate loads.
- Ultimate tip deflection shows an increase when the Wake redirection is im-

plemented alone, on the contrary, derating has the opposite effect already for down-regulations below 5%.

- Fatigue loads are less affected, considering the WFC will not be active during the entire lifetime of the turbine.
- As expected, power production is reduced for all configurations.

The results show that pairing the two strategies could be advantageous, in fact the increase in tip deflection given by WR would demand a blade redesign in order to withstand the higher loading, which converts in an increased blade mass and cost, as well as not being feasible for already existing wind farms. This step could be avoided by implementing derating on the WFC and imposing a reduction between 0.5% and 6%, depending on the yaw angle needed, which is lower than the overall power production increase promised by WR. Higher values of derating show diminishing returns on the reduction in the blade's loads and tip displacement, and since the main purpose of the down-regulation is to counter the downsides of yaw steering, they are not convenient, besides considering the consequent loss in production for the operating turbine and at the farm level, because the induction control is reserving energy inside a wake that is not investing any turbine if WR has been implemented correctly.
While tip deflection is most of the times the main constraint in the design process, the large increase in ultimate loads for tower and hub when yaw steering is in play might break safety boundaries for the respective components. In that case a structural redesign of either component is necessary, since in this case the addition of derating is not enough to counter the effects of the yaw misalignment. Alternatively, one could limit the maximum yaw angle to avoid extreme cases.
It is also important to note that, as already mentioned, the simulation have been performed following certification procedures for single turbines because of the lack of dedicated standards for wind farm design in order to have a consistent methodology to apply to all configurations under study, such that the results are comparable. As a possible future development of this work it could be interesting to repeat this study once certification requirements at the wind farm level are defined to have more realistic results or to study how and whether to change the current regulation guidelines to cover these aspects. Also, the effects of the combination of WR and derating here proposed could be tested on different turbine designs, such as lower power turbines that are already installed in modern wind farms and are commercialized or in the case of different materials like carbon blades, where the main design constraint is not the ultimate tip displacement and the structural behavior of the system is quite different with respect to fiber glass blades.
Another possible development is to study whether the two strategies combined

increase the wind farm efficiency as expected or not, possibly for different wind farm configurations. Finally, a more refined set of configurations may be tested, especially for low percentages of derating, in fact, the results from this project show that the effect of induction control on the blade's ultimate loads and tip displacement is great already at low values of the reduction, while at 10% or higher it's even too much in reducing the loads, considering the detrimental loss in production.

Appendix A

Results of the ranking analysis on the baseline model

Here we present and briefly discuss the results from the ranking analysis mentioned in chapter 3 to give context to the choice to exclude some DLC's from the parametric analysis on the two wind farm control strategies.
Starting from the blade flapwise ultimate loads, fig. A.1 represents the top 20 DLC's for this particular load. As can be noted DLC 1.5 makes an appearance, but with much lower impact compared to DLC 1.3 and 1.4. Even DLC 1.1 experiences an higher flapwise moment during the simulation at $11m/s$.

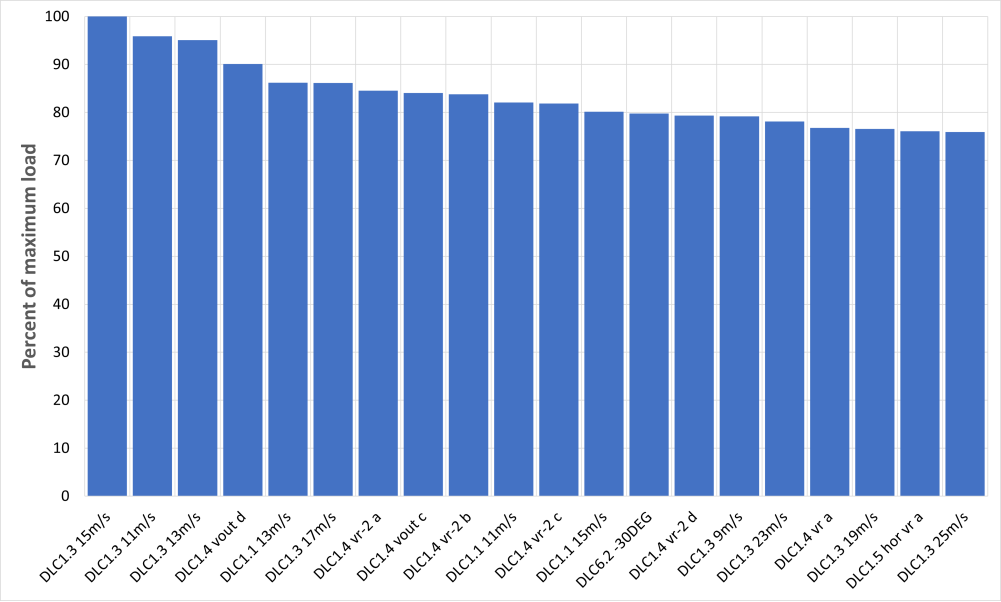

Figure A.1: *Ranking for blade flapwise moment.*

Then the DLC's that gave the highest value for tip deflection are illustrated in fig. A.2. Again, the most important values come from DLC 1.3 and 1.4, but this time the extreme wind shear is more represented. However the impact is still relatively low compared to the other two (and also DLC 1.1).

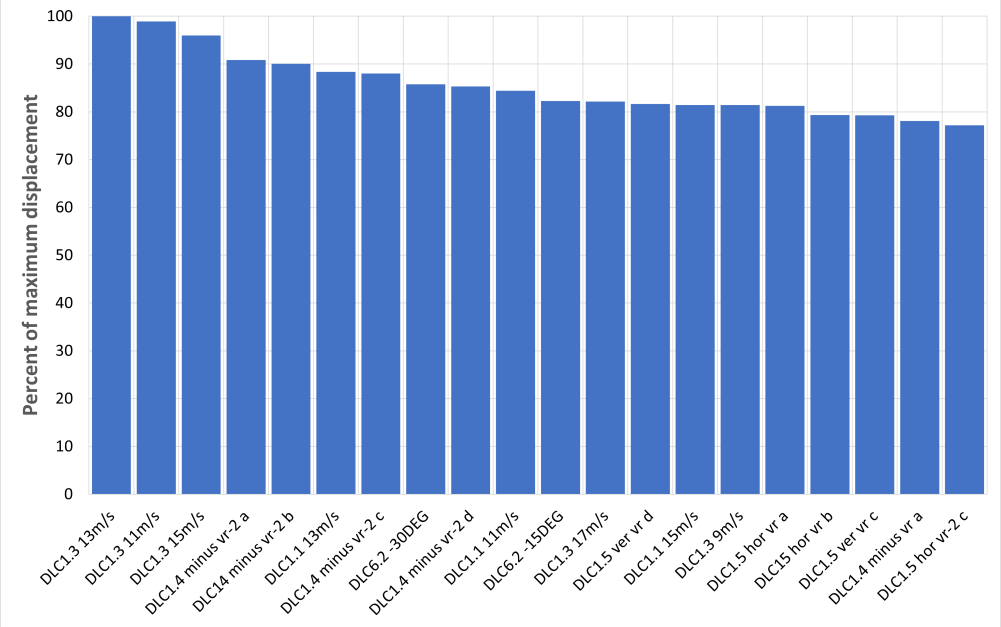

Figure A.2: *Ranking for maximum tip deflection.*

Following that we performed the same analysis for both the tower top and tower base fore-aft. side-side and combined moment. Figures A.3 and A.4 show the top 20 DLC's from respectively tower top and base. In this case DLC 1.4 and 2.3b are the most represented, followed by 2.2f and 6.2. Finally DLC 2.2a makes an appearance on the tower top ranking, however with a maximum value which is slightly above 70% of the ultimate load registered and is clearly outclassed by the pitch runaway failure of DLC 2.2f, which is strictly worse than the pitch freeze.

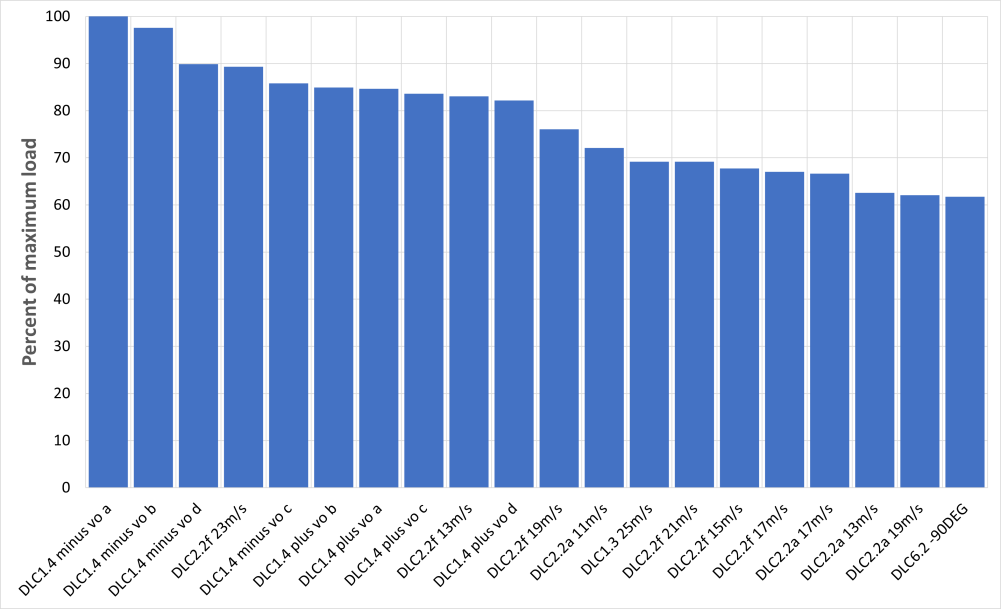

Figure A.3: *Ranking for tower top combined moment.*

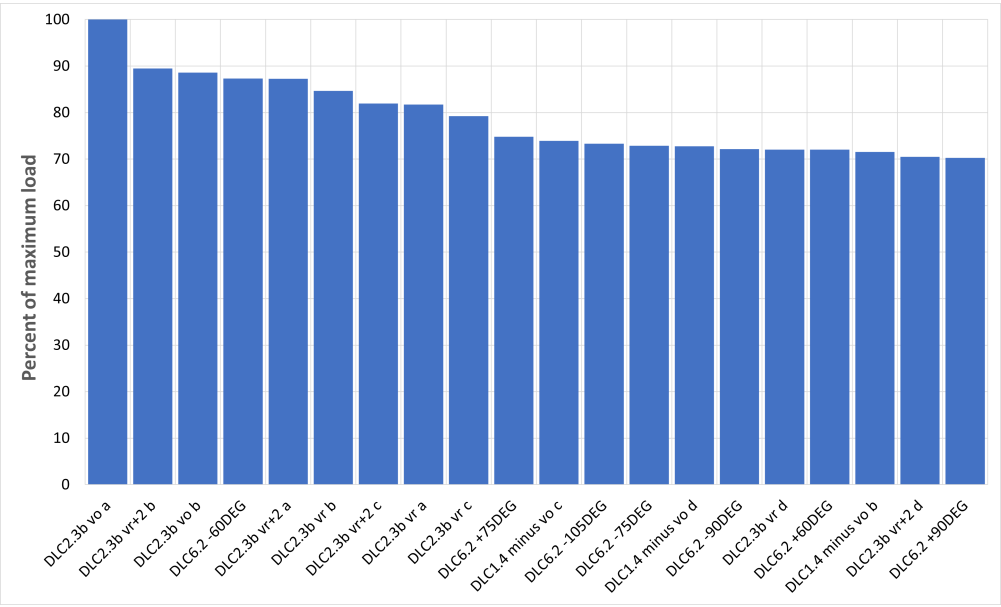

Figure A.4: *Ranking for tower base combined moment.*

Lastly, fig. A.5 shows the ranking analysis for the hub combined moment. DLC 1.4 demonstrates once again his importance in the load envelope of the wind turbine, followed by DLC 2.2f, which is already below 90% of the maximum load. DLC 2.2a appears two times, near the end of the rankings.

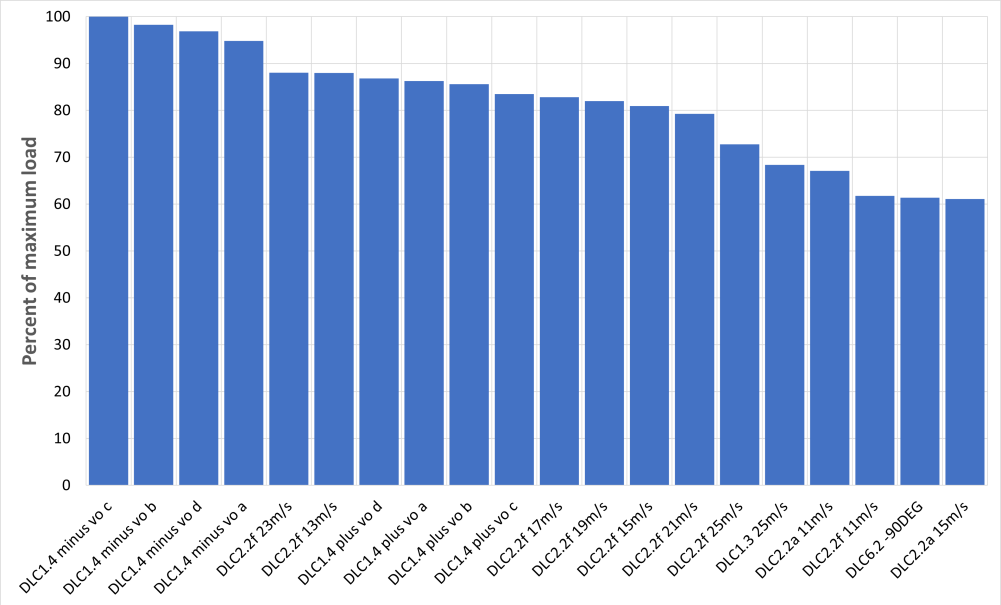

Figure A.5: *Ranking for hub combined moment.*

As stated in chapter 3, we decided to exclude DLC 1.5 and 2.2a from the parametric analyses which would test the behaviour of the two wind farm control strategies combined. In fact from the results here presented it can be seen the relatively low importance of both DLC's on the ultimate loads. Although DLC 2.2b does not show up in this analysis, we initially opted to keep it during the parametric analysis, due to the different kind of failure with respect to the pitch runaway. In hindsight, it would have been better to exclude it too, since it does never appear as ultimate load in the results presented in chapter 4.

Bibliography

[1] Irena (2019). *Future of wind: Deployment, investment, technology, grid integration and socio-economic aspects (A Global Energy Transformation paper)*. International Renewable Energy Agency, Abu Dhabi.

[2] WindEurope. *Annual Statistics*. 2018. URL: https://windeurope.org/wp-content/uploads/files/about-wind/statistics/WindEurope-Annual-Statistics-2018.pdf.

[3] Soo-Hyun Kim et al. "A study of the wake effects on the wind characteristics and fatigue loads for the turbines in a wind farm". In: *Renewable Energy* 74 (Feb. 2015).

[4] R. Barthelmie et al. "Modelling the impact of wakes on power output at Nysted and Horns Rev". In: *European Wind Energy Conference and Exhibition 2009, EWEC 2009* 2 (Jan. 2009).

[5] Tony Burton et al. *Wind Energy Handbook*. 2011.

[6] Christian Santoni, Umberto Ciri, and Mario Rotea. "Development of a high fidelity CFD code for wind farm control". In: *Proceedings of the American Control Conference* 2015 (July 2015), pp. 1715–1720.

[7] Mike Dijk et al. "Yaw-Misalignment and its Impact on Wind Turbine Loads and Wind Farm Power Output". In: *Journal of Physics: Conference Series* 753 (Sept. 2016).

[8] Alessandro Croce et al. *Evaluation of the impact of wind farm control techniques on fatigue and ultimate loads*. Feb. 2020.

[9] C. Bak et al. *The DTU 10MW Reference Wind Turbine*. 2013.

[10] J.Å. Dahlberg and S.E. Thor. *Power performance andwake effects in the closely spaced Lillgrund offshore wind farm*. European Offshore Conference, Stockolm, 2009.

[11] CL-Windcon. *Minimal loading wind turbine de-rating strategy and active yaw controllers*. 2017.

[12] G P Corten and P Schaak. *Heat and Flux. Increase of Wind Farm Production by Reduction of the Axial Induction*. Oct. 2003.

[13] Jan Bartl and Lars Sætran. "Experimental testing of axial induction based control strategies for wake control and wind farm optimization". In: *Journal of Physics: Conference Series* 753 (Sept. 2016).

[14] Paul Fleming et al. "Initial Results From a Field Campaign of Wake Steering Applied at a Commercial Wind Farm: Part 1". In: *Wind Energy Science Discussions* (Feb. 2019), pp. 1–22.

[15] Pieter Gebraad et al. "Wind plant power optimization through yaw control using a parametric model for wake effects—A CFD simulation study". In: *Wind Energy* (Dec. 2014).

[16] Paul Fleming et al. "Simulation comparison of wake mitigation control strategies for a two-turbine case". In: *Wind Energy* 18 (Oct. 2014).

[17] Jesse Wang, Carlo Bottasso, and Filippo Campagnolo. "Wake redirection: comparison of analytical, numerical and experimental models". In: *Journal of Physics: Conference Series* 753 (Sept. 2016).

[18] Jay Goit and Johan Meyers. "Optimal control of energy extraction in wind-farm boundary layers". In: *Journal of Fluid Mechanics* 768 (Apr. 2015), pp. 5–50.

[19] Wim Munters and Johan Meyers. "Towards practical dynamic induction control of wind farms: analysis of optimally controlled wind-farm boundary layers and sinusoidal induction control of first-row turbines". In: *Wind Energy Science Discussions* (Feb. 2018).

[20] Stefano Cacciola et al. *A CFD-Based Analysis of Dynamic Induction Techniques for Wind Farm Control Applications*. Feb. 2021.

[21] J. Jonkman et al. *Definition of a 5-MW Reference Wind Turbine for Offshore System Development*. NREL, Feb. 2009. URL: `https://www.nrel.gov/docs/fy09osti/38060.pdf`.

[22] Mark Drela. "XFOIL: An Analysis and Design System for Low Reynolds Number Airfoils". In: vol. 54. June 1989.

[23] Christian Bak, Jeppe Johansen, and Peter Andersen. "Three-Dimensional Corrections of Airfoil Characteristics Based on Pressure Distributions". In: (Jan. 2006).

[24] M.H. Hansen and L.C. Henriksen. *Basic DTU Wind Energy Controller*. DTU Wind Energy, Denmark, 2013.

[25] *OpenDiscon*. 2017. URL: `https://github.com/ielorza/OpenDiscon`.

[26] Carlo Bottasso and Alessandro Croce. *Power Curve Tracking with Tip Speed Constraint using LQR Regulators*. Apr. 2009.

[27] Carlo Bottasso et al. "Aero-servo-elastic modeling and control of wind turbines using finite-element multibody procedures". In: *Multibody System Dynamics* 16 (Oct. 2006), pp. 291–308.

[28] B. Jonkman and B. Jr. *TurbSim User's Guide*. 2007.

[29] International Electrotechnical Commission. *IEC 61400-1 Wind Turbines - Part 1: Design Requirements*. 2006.